CONF-9206332--1

Electronic Structure Studies of $YBa_2Cu_3O_x$ ($6.2 \leq x \leq 6.9$) using Angle Resolved Photoemission*

B. W. Veal, Rong Liu, A. P. Paulikas, D. D. Koelling, Hao Shi,** and J. W. Downey
Materials Science Division and Science and Technology Center for Superconductivity Argonne National Laboratory, Argonne, IL 60439

C. G. Olson
Ames Laboratory and Department of Physics Iowa State University, Ames, IA 50011

A. J. Arko, J. J. Joyce and R. Blythe
Los Alamos National Laboratory, Los Alamos, NM 87545

ANL/MSD/CP--77995

DE93 004811

November 1992

INVITED PAPER presented at the Tenth International Summer Institute in Surface Science (ISISS), Milwaukee, Wisconsin, June 29–July 2, 1992. Proceedings to be published in a special issue of *Surface Science Reports*.

*Work at Argonne National Laboratory is supported by the U.S. DOE under contract #W-31-109-ENG-38 (BWV,APP,HS,JWD) and by the NSF, Science and Technology Center for Superconductivity, under contract #DMR 8809854 (RL). Ames Laboratory is operated for U.S. DOE by Iowa State University under contract #W-7405-ENG-82. The Synchrotron Radiation Center is supported by NSF under contract #DMR 8601349.

**Present Address: Department of Physics, University of Missouri, Kansas City, MO 64110.

Electronic Structure Studies of $YBa_2Cu_3O_x$ ($6.2 \leq x \leq 6.9$) using Angle Resolved Photoemission

B. W. Veal, Rong Liu, A. P. Paulikas, D. D. Koelling,
Hao Shi,* and J. W. Downey
Materials Science Division and
Science and Technology Center for Superconductivity
Argonne National Laboratory, Argonne, IL 60439

C. G. Olson
Ames Laboratory and Department of Physics
Iowa State University, Ames, IA 50011

A. J. Arko, J. J. Joyce and R. Blythe
Los Alamos National Laboratory, Los Alamos, NM 87545

ABSTRACT

Using high resolution angle resolved photoemission, the electronic structure of $YBa_2Cu_3O_x$ is examined when oxygen stoichiometries are varied in the range $6.2 \leq x \leq 6.9$. Detailed measurements of the Fermi surface for $YBa_2Cu_3O_{6.9}$ are presented and are compared with predictions of band theory. In the metallic region of the phase diagram, changes in the Fermi surfaces are measured as a function of oxygen stoichiometry. The electronic structure is monitored as the oxide changes from a metal to a semiconductor with additional oxygen depletion. For intermediate stoichiometries, effects of oxygen vacancy ordering are considered. Unusual resonant effects observed at several photon energies are examined as oxygen content is varied.

---

* Present Address: Department of Physics, University of Missouri, Kansas City, MO 64110.

I. INTRODUCTION

Essential to the development of a suitable description of the superconducting state in high T_c oxides is a clear understanding of the normal state electronic properties. A very basic issue is whether the normal state can be described by Fermi liquid (FL) theory [1-4]. The possibility of strong electron correlation effects has led to widespread skepticism about the appropriateness of FL theory to describe the normal state in the copper oxide superconductors. Indeed, high T_c oxides show many properties that are considered to be anomalous [4] and are frequently cited as demonstrating the failure of FL theory for these materials [5].

While early debate on this issue centered on a discussion of whether or not a Fermi surface (FS) exists in these metallic oxides, recent angle resolved photoemission (ARPES) [6-12], positron annihilation (PAS) [13-14], and de-Haas-van Alphen (dHvA) [15-16] measurements have provided strong evidence for the existence of a Fermi surface in $YBa_2Cu_3O_x$. Fermi surface measurements have been reported for other high T_c oxides as well.

Since band calculations (local density approximation) provide a very detailed specification of allowed electron energy states including those low energy states that define the Fermi surface, the calculations have been frequently tested by comparison with experiment. And, in general, reported FS measurements show relatively good correspondence with Fermi surfaces predicted from band theory [3]. However, band theory appears to be inappropriate for the insulating, oxygen deficient $YBa_2Cu_3O_6$. Band theory predicts metallic behavior [17-18] even though $YBa_2Cu_3O_6$ is an antiferromagnetically ordered insulator with magnetic moments localized on Cu sites [19] .This failure of local density theory is

also encountered with other (parent) insulating oxides which become superconducting with suitable doping. The Hubbard Hamiltonian has been widely used to describe the insulator and doped insulator regimes.

Since the extremes of the $YBa_2Cu_3O_x$ phase diagram show strongly contrasting properties, perhaps requiring rather different theoretical machinery to describe the endpoints, it is important to investigate the electron states in high T_c oxides as the materials are transformed from the metallic (superconducting) into the insulating state. In this paper, we report such a study, probing occupied electron states of $YBa_2Cu_3O_x$ as oxygen stoichiometry is varied between metallic and insulating regimes. We report ARPES studies of $YBa_2Cu_3O_x$, with oxygen content varied in the range $6.2 \leq x \leq 6.93$, with emphasis on identifying and measuring Fermi surfaces and monitoring FS changes as x is varied. Varying the oxygen stoichiometry produces changes in the carrier concentration and in the superconducting T_c. We explore the effect of this stoichiometry variation on the Fermi surface and study the transition into the insulating state as oxygen content is reduced. Effects of oxygen vacancy ordering are also considered. While it has long been known that vacancy ordering occurs in oxygen deficient YBCO [20], it has only recently been demonstrated that the state of order has a profound effect on both superconducting and normal state properties [21]. We also examine the unusual resonant effects that are observed at certain photon energies and emission angles and their behavior as the material transforms from the metallic to the insulating state with oxygen depletion.

The paper is organized to include a discussion of (1) experimental considerations involved in the ARPES measurements, (2) the crystallographic structure of YBCO including effects of chain vacancy ordering,

(3) a brief discussion of band calculations, (4) ARPES Fermi surface measurements in $YBa_2Cu_3O_{6.9}$ and in oxygen deficient samples, (5) observed resonant features, and (6) ARPES measurements in the vicinity of the metal-insulator transition.

II. EXPERIMENTAL CONSIDERATIONS

Single crystals were grown in gold crucibles from a Cu and Ba rich mixture (a "self-flux" procedure). Oxygen stoichiometries in the range $6.2 < x < 6.85$ were fixed by equilibrating the samples at 520°C in an appropriate mixture of oxygen and nitrogen gases [21]. After equilibrating for several days, samples were quenched to liquid nitrogen. Using this procedure, any desired T_c could be readily obtained with a sharp superconducting transition. Determined from SQUID magnetization measurements, ΔT_c's are routinely less than 2 K wide (10 and 90 % values). To obtain a "fully oxygenated" sample, estimated to have stoichiometry 6.93, samples were annealed at 480°C for about one week followed by a second anneal of comparable duration at 420°C. Figure 1 shows a plot of T_c vs oxygen depletion for a series of single crystal measurements. Stoichiometries were determined from a calibration established by iodometric titration on ceramic samples that were concurrently processed with single crystal samples [22]. Samples used in these studies were thin platelets of typical dimensions 1 x 1 x 0.1 mm^3. The samples were cleaved in the vacuum system (~4 X 10^{-11} Torr) of the ARPES spectrometer, to expose an a-b surface, after cooling to about 20 K. Measurements were taken with the sample temperature maintained near 20 K. If measurements are taken at room temperature, significant time dependent changes

occur indicating oxygen depletion at the sample surface or severe surface reconstruction [23].

ARPES measurements for Fermi surface studies were made on the Ames-Montana ERG-Seya beamline at the Synchrotron Radiation Center at Stoughton, WI, using the Seya monochromator with photon energies in the 15-30 eV region. The angular resolution of the electron analyzer is 2° (full apex acceptance cone) which corresponds to a k-resolution of 0.07 A^{-1} (about 1/11 of the Γ-to-X distance in k-space) for $h\nu$ = 21.2 eV. The total (photon plus electron) energy resolution was 55 meV. Some of the resonant features were measured using higher resolution conditions (20-30 meV resolution). Data were also acquired, for photon energies exceeding 30 eV, at the Los Alamos ERG beamline at the National Synchrotron Light Source at Brookhaven National Laboratory, NY. See references [6,7] for more details pertaining to measurement conditions, including sample orientations with respect to photon beam polarization.

Use of the ARPES technique is most straightforward when the material under study has a highly two-dimensional structure with band dispersion occurring only in a plane parallel to the sample surface. This condition appears to be nicely satisfied for cleaved surfaces of YBCO. Cleaving exposes the a-b plane where dispersion is large; c-axis dispersion is apparently very small. However, complicating the experimental situation is the fact that ARPES is a very surface sensitive technique. Electron escape depths for photoelectrons ejected from E_F are of the order of one or two unit cells when $h\nu \sim$ 15-30 eV (photon energies most extensively used in this study). Consequently, spectra could be significantly influenced by the presence of the sample-vacuum interface; surface relaxation, surface

reconstruction or charge redistribution might occur in the near-surface region perturbing the underlying bulk electronic structure [24].

III. STRUCTURE

YBCO has an orthorhombic structure in the superconducting phase and transforms to a tetragonal structure when $x \leq 6.4$ [22] where it becomes an antiferromagnetic insulator [25]. Figure 2 shows the structure of the perfect $YBa_2Cu_3O_7$ material. Pairs of CuO_2 planes separated by a layer of Y atoms are generally believed to be the essential component of the structure for sustaining superconductivity. These planes, with Cu atoms in 4-planar coordination to neighboring oxygens are common to all of the high T_c Cu-oxide superconductors. Layers containing Cu-O chains also appear in the YBCO structure. The chains, when fully occupied, also contain Cu's in four-coordination. However, oxygens in the chains are relatively weakly bound; when the oxygen stoichiometry is reduced, oxygen vacancies appear in this portion of the structure. All of the oxygens in the O(1) sites [22] of the chain layer can be removed without sample decomposition. As oxygen is removed, the coordination number of chain Cu's is decreased; with sufficient oxygen removal, these Cu(1) sites become 2-coordinated.

IV. CHAIN VACANCY ORDERING

Oxygen vacancies in the chain basal plane have a strong tendency to order, forming long chains in the b-direction. These strings of vacancies also tend to order in the a-direction. When $x = 6.5$, for example, alternate filled and empty chain sites are observed forming the Ortho II structure [20]. It was discovered, however, that disorder could be thermally

introduced into this layer of the structure, with profound effect on both superconducting and normal state properties [21,26-28]. When disorder was introduced (by annealing and quenching experiments), relaxation (ordering) occurred, even at temperatures as low as room temperature.

Figure 3 shows a series of a-b plane resistivity measurements $\rho(T)$ on a $YBa_2Cu_3O_{6.41}$ single crystal sample prepared with quenched-in disorder [29]. After fixing the oxygen stoichiometry, leads were attached and the sample was given a secondary anneal at 180°C, a temperature sufficiently high to introduce substantial disorder into the chain basal plane. The sample was then quenched to a chilled solution of Fluorinert (a commercial quenching fluid) to preserve the disorder. The upper curve in Fig. 3, showing semiconducting behavior, was measured immediately after quenching. Repeated $\rho(T)$ measurements were taken after permitting the sample to anneal at room temperature for the specified time intervals. With room temperature annealing, the normal state resistivity falls and the material converts to a superconductor. With extended room temperature annealing of this $YBa_2Cu_3O_{6.41}$ sample, T_c rises and saturates at about 20 K.

This aging behavior was explained as a "hole doping" phenomenon resulting from changing copper coordinations in the chain basal plane [30-32]. Figure 4 shows a representation of the chain basal plane for $YBa_2Cu_3O_{6.5}$, where the large dots represent oxygen atoms and the small dots represent copper atoms. In Fig. 4, most of the oxygen atoms are arranged to define the Ortho II structure but some O's are shifted (i.e., are thermally driven) to normally vacant chain sites. As these misplaced O's move back into their Ortho II sites (with low temperature annealing), they increase the number of two-coordinated Cu's. Two-coordinated Cu's,

bonded to neighboring oxygen, are normally monovalent species. If the three-and four-coordinated Cu's are nominally divalent, then this annealing process sequesters or freezes-out electrons by creating Cu^{1+} sites thus increasing the hole concentration in the material (a p-type conductor).

Profound changes in the normal state and superconducting properties are caused by changing oxygen stoichiometry and by altering the state of order in the chain basal plane. It appears that, in both cases, the properties changes are attributable to changes in carrier concentration. Since changes in the carrier concentration should also appear as changes in Fermi surface dimensions, we expect that variations in oxygen stoichiometry as well as variations in the state of oxygen vacancy order will alter the size of the Fermi surface. In this paper, we report Fermi surface studies, on samples well annealed at room temperature, with their oxygen concentrations varied between 6.2 - 6.9. Measurements with varied states of order have not yet been undertaken. If such experiments could measure Fermi surface changes, they should provide important insight into the question of charge redistribution associated with order induced hole doping. Information might also be gained about surface relaxation effects; vacancy ordering might be somewhat different in the near vicinity of the vacuum interface.

V. BAND CALCULATIONS

Figure 5 shows the band structure, from a calculation by Massidda, et al. [33], for $YBa_2Cu_3O_7$. The band structure is exceedingly complicated for electron binding energies greater than a few tenths of an eV. Near E_F, however, bands are relatively simple, so that, with high resolution ARPES

capability, band dispersion and Fermi surfaces might be observed and meaningfully analyzed. In Fig. 6a, we show the Brillouin zone section in the reduced zone scheme (Γ corresponds to the zone center). Figure 6b shows an overlay of Fermi surfaces calculated [33] at $k_z = 0$ (i.e., in the plane containing Γ) and at $k_z = \pi/c$ (in the plane containing Z). The shaded regions connect surfaces from common bands that appear in the two planes. The width of these shaded regions provide an indication of the k_z band dispersion; k_z dispersion is small when the indicated regions are narrow. The regions labeled 1 and 4 (corresponding to bands 1 and 4 in Fig. 5), are Fermi surfaces from bands that have a substantial (or dominant) admix of chain band character. The shaded regions (labeled 2 and 3) are predominantly plane-band derived.

Figure 6c shows another Fermi surface calculation, from Pickett, et al. [34]. A calculation by Andersen et al. [35] yields very similar results to this calculation. Indeed, overall agreement among all the reported band structures, of which these are only a representative sampling, is very good. There are three sensitive Fermi surface features where differences appear: (a) the hole appearing in the chain band surface (band 1) at the point U; (b) the bulge or protrusion towards the Γ-Y line (or necking across) by the band 2 surface which results from the CuO_2 plane states that give rise to the "barrels" interacting with chain states; and (c) the size of the chain band (4) surface along the S-R line. All of these sensitivities are dramatically influenced by the positioning of the chain bands relative to the plane bands and by the details of their interactions. Very small energy shifts can cause these changes; for example, the difference at the U point (Fig. 6b and 6c) corresponds to a shift of only 0.04 eV. Nonetheless, these changes have significant physical consequences and so should be probed.

In the region of the bulge (band 2), there is substantial hybridization between chain and plane derived bands. Since we are examining oxygen variation in YBCO, where oxygen is removed from chain sites, we might expect the predominately chain derived bands (labeled 1 and 4 and the bulge in band 2) to show the greatest sensitivity to stoichiometry variation.

We note that electronic structures of the reduced stoichiometry ordered phases can also be calculated using band theory or other theoretical procedures which require a detailed knowledge of atomic structure. In addition to band calculations for the endpoint stoichiometries $YBa_2Cu_3O_7$ and $YBa_2Cu_3O_6$, calculations are now available for the ordered (Ortho II) phase of $YBa_2Cu_3O_{6.5}$ [31,36].

VI. ARPES MEASUREMENTS - FERMI SURFACE of $YBa_2Cu_3O_{6.9}$

ARPES measures energy distribution curves (EDC's) of photoelectrons emitted into a small solid angle. These EDC's provide an approximate measure of the occupied electronic density of states in a small window of k-space. We measure a series of EDC's along a chosen direction in k-space and look for spectral features that disperse toward E_F. An abrupt drop in intensity occurs when the dispersing feature moves through the Fermi level. The point in k-space where the band crosses the Fermi level defines a point on the Fermi surface. Figure 7a shows a series of EDC's for the "fully oxygenated" x = 6.9 sample taken along the Brillouin zone diagonal, $\bar{\Gamma}$-$\bar{S}$ (the measurements are actually taken along a line somewhere between Γ-S and Z-R that is approximately parallel to the large faces of the Brillouin zone; k_z is not well defined). Note, in Fig. 7a, that a spectral feature appears near 0.3 eV when the electron pickoff angles $\theta = \phi = 4°$.

This feature disperses toward E_F, crossing the Fermi level at about $\theta = \phi = 9°$, where an abrupt dropoff in intensity occurs. While this intense dispersing feature is clearly observed in the data, a second, poorly defined, spectral feature may also appear as a shoulder on the low binding energy side. This feature is indicated by an arrow on the EDC at $\theta = \phi = 6°$. We conclude that this feature passes through E_F near $\theta = \phi = 7°$. To assist with this band identification, we include, in Fig. 7b, a series of EDC's from $Bi_2Sr_2CaCu_2O_8$, believed to correspond to a single dispersing band [37]. Note that no shoulder is apparent in the EDC as the spectral feature approaches E_F.

By examining EDC's measured on a grid covering every two degrees in θ and ϕ, we map dispersing bands throughout the entire first Brillouin zone. (All of these measurements were taken at $h\nu = 21.2$ eV.) Arranging these EDC's along different directions, we follow band dispersions and map Fermi level crossings to obtain redundant measurements of the Fermi surface [6,7]. Results are shown as solid and open circles in Fig. 8; the solid circles are those determined with greatest clarity. Results are compared with the Fermi surfaces calculated by Pickett et al [34]. Most of the solid dots apparently correspond to the plane-related Fermi surface that is labeled 3 in Fig. 8. The open circles are somewhat more subjective, corresponding to spectral features that are less clearly defined, as discussed above. Since measurements were taken on twinned samples, it is not known if the observed bulge near θ or $\phi = 15°$ should be associated with $\bar{\Gamma}$-$\bar{X}$ or $\bar{\Gamma}$-$\bar{Y}$ symmetry directions. With the possible exception of those points near θ or $\phi = 15°$, Fig. 8 does not show a clear measurement of Fermi surfaces that have dominant chain band character.

In contrast with previous ARPES studies [9], we do not observe the small chain related hole pocket predicted to occur near the S point [6]. (Note, however, that both PAS and dHvA measurements have also been attributed to this small surface). In general, correspondence between the predictions of band theory and the observed Fermi surfaces is good.

VII. FERMI SURFACE - VARIED OXYGEN STOICHIOMETRY

Next we examine Fermi surfaces when the oxygen stoichiometry is reduced below 6.9. Figure 9 shows a comparison of EDC's taken along the $\bar{\Gamma}$-$\bar{S}$ line for the 6.9 and 6.5 samples. Apparently, the inner plane band (band 3, Fig. 8) is not strongly affected by changes in oxygen stoichiometry when $x \geq 6.4$ [6,7]. Figure 10 shows a similar comparison of EDC's along the $\bar{\Gamma}$-$\bar{Y}(\bar{X})$ symmetry line for the x = 6.9 and 6.5 samples. (Note that these samples are twinned, so a superposition of spectra from $\bar{\Gamma}$-$\bar{X}$ and from $\bar{\Gamma}$-$\bar{Y}$ is measured.) Now we observe a significant stoichiometry-dependent difference in the spectra. In Fig. 10a, a spectral feature moves to, and apparently through, the Fermi level where spectral intensity is abruptly lost when θ and ϕ are near 16°. When x = 6.5, similar band dispersion can be discerned, but there is a dramatic change in the spectral weight near E_F. It is not clear, furthermore, that a Fermi level crossing can be convincingly identified. Thus, there appear to be discernible changes in the Fermi surface, with oxygen depletion, in the vicinity of the $\bar{\Gamma}$-$\bar{Y}(\bar{X})$ symmetry lines. This may signal changes in the chain bands (band 1 and/or band 4 -- see Fig. 6b).

These observations again appear to be consistent with predictions from band theory for the double-cell (Ortho II) $YBa_2Cu_3O_{6.5}$ composition.

Figure 11 shows the calculated Fermi surface that is cut by one plane (containing Γ) of the Brillouin zone [6, 35]. Note that the surfaces from plane bands 2 and 3 persist relatively unchanged from their corresponding surfaces in Fig. 6. (Small modifications occur near the new zone boundary; bands 2' and 3' are plane bands which appear as a consequence of cell doubling.) Chain band 1 persists, somewhat modified, but it is not doubled in the new cell; i.e., one chain layer has been removed relative to the x = 7 structure. Thus we might expect to observe a loss of chain band intensity as the oxygen stoichiometry is reduced. Further, band 4 (see Figs 5 and 6) no longer crosses E_F. In general, these predicted changes appear to be consistent with the changes in ARPES spectra observed between the x = 7 and x = 6.5 samples. With oxygen depletion, spectral intensity and possibly a Fermi level crossing are lost near BZ edges.

With the formation of the Ortho II structure, a new periodicity occurs. In the new (x = 6.5) Brillouin zone, the Γ - X distance is about half of the Γ - X distance for the x = 7 structure. Since reflection symmetry occurs about the line X - S (Fig. 11), band re-entrant behavior should appear in the second zone of the new cell. As seen in Fig. 9b, there is no indication in the spectra for the new periodicity, i.e.., the spectra do not show symmetry with respect to the new zone boundary. It may be that the states being probed (primarily plane related) are not dramatically perturbed by the new periodicity so that the effect of cell doubling can not be observed at this level of sensitivity [6]. Furthermore, we do not see evidence for the new structure (bands 2' and 3') along Γ - Y in the first zone.

VIII. RESONANT FEATURES

In $YBa_2Cu_3O_x$, there are a number of sharp and intense spectral features which appear at specific photon excitation energies and at specific points or regions in the Brillouin zone. (We refer to these unusual spectral structures as resonant features. Tobin et al. [10] call them acute features.) Such features appear very prominently at 17 eV at the $\bar{Y}$ -point, 24 eV at $\bar{X}$ and $\bar{Y}$, 28 eV at $\bar{Y}$, and 74 eV at $\bar{X}$ and $\bar{Y}$. The 17 and 28 eV features are most prominently peaked at E_F while the 24 and 74 eV features appear most intensely at about 1 eV binding energy [6-8,10,38]. (These features can be used to great advantage in confirming sample alignment for ARPES measurements.) The origin of these features has not been firmly established, whether they might be surface states, band structure features, or another type of excitation. The 17 eV feature, which appears at E_F at the $\bar{Y}$ - point in the Brillouin zone, was discovered by Tobin et al [10] in an $x = 6.9$ sample. The behavior of this feature is nearly identical to that shown in Fig. 12 for an $x = 6.5$ sample. The feature appears to be nondispersive and is extremely sharp, displaying a 20 meV FWHM peak, essentially a measure of the instrument resolution function. For oxygen stoichiometries where the sample is superconducting, the feature appears to be relatively insensitive to oxygen variation.

Another feature appears prominently at E_F at the $\bar{Y}$ -point of the zone when $h\nu = 28$ eV. This feature, shown in Fig. 13 for $x = 6.5$, also appears to be insensitive to oxygen variation when the sample is metallic [6,7,10]. The 28 eV peak clearly shows dispersive behavior. One might attribute this feature to band 2 (see Figs 5 and 6), in which case the band approaches (or just crosses) E_F along the $\bar{\Gamma}$-$\bar{Y}$ line [39]. The relative insensitivity of this

band to oxygen variation also appears to be consistent with the Ortho II calculation which shows that the band remains very close to E_F along $\bar{\Gamma}$-$\bar{Y}$ although it doesn't cross [36]. As discussed above, relative loss of spectral weight might be expected when x = 6.5 since chain band states are lost in the reduced sample.

The resonant features at 17 and 28 eV may, in fact, be sensitive to the same occupied electron states [40]. Dispersion, apparent in the 28 eV spectra (Fig. 13), is not observed when hν = 17 eV since the intensity is sufficiently strong to clearly define the feature only in a small region of k-space near the $\bar{Y}$ point. A second peak in Fig. 12, appearing near 0.1 eV at $\bar{Y}$, disperses toward E_F along the $\bar{Y}$-$\bar{S}$ direction. Note that bands 3 and 4 in the band calculation of Fig. 5 show similar behavior.

The 1 eV resonant feature at 24 eV photon energy apparently reappears at 74 eV. EDC's are shown, in Fig. 14, along the $\bar{\Gamma}$- $\bar{Y}(\bar{X})$ line measured using 24 and 74 eV photon energies [41]. Note that the 1 eV feature shows similar dispersive behavior and comparable intensity variations for k-values in the range 0.5 - 0.9 A^{-1}. However, the intense peak near 1.5 eV observed at the $\bar{\Gamma}$ point when hν = 24 eV binding energy is absent in the hν = 74 eV EDC's. It may be that the 1 eV peak at 74 eV is enhanced by the coupled excitation between Cu 3p and empty Cu 3d states which also occurs at 74 eV. Since the enhancement is largest when 3d valence band states are also involved (in a super Coster-Kronig autoionization process), the suggestion is that the 1 eV resonant feature at $\bar{Y}(\bar{X})$ involves valence band states that contain a significant admix of Cu 3d character. (Note that valence band satellites also show resonant behavior at hν = 74 eV suggesting that strong correlation effects occur in the Cu 3d band [23]).

Since the 1 eV resonant peak occurs at both $\bar{X}$ and $\bar{Y}$, it seems likely that the feature is associated with plane derived electron states. The chain layer is highly anisotropic and the anisotropy varies with x; the planes show little anisotropy at all oxygen stoichiometries. (In contrast, the $h\nu$ = 17 and 28 eV features appear only at $\bar{Y}$, which suggests association with the chain layer.) The 1 eV resonant behavior at $h\nu$ = 24 eV might result from enhancement involving a coupled Y 4p→Y 4d and/or O 2s→O 2p absorption. A 1.5 eV peak also appears at $\bar{\Gamma}$ (Fig. 14) with substantial intensity when $h\nu$ = 24 eV. However, its resonance properties have not yet been carefully examined. Additional measurements, including studies on $RBa_2Cu_3O_x$ crystals with the R element a lanthanide (replacing the Y 4p core level with a Ln 5p) are needed to help clarify interpretation of these results.

Strong intensity modulations of ARPES spectra also appear as a function of k when YBCO valence band states are measured in higher Brillouin zones. For example, Fig. 15 shows a series of EDC's, with $h\nu$ = 74 eV, taken along the $\bar{\Gamma}$-$\bar{X}$($\bar{Y}$) directions (twinned sample), scanning through several Brillouin zones. At the Fermi level, a strong, zone dependent, intensity modulation is observed. Note, especially, in the range $\bar{\Gamma}''$-$\bar{X}''$, that the peak at E_F becomes very intense. The EDC for k = 3.67 A^{-1}, where the peak at E_F is maximum, is reproduced in Fig. 16. Other k-dependent modulations of spectral features are also apparent throughout the valence band. The 1 eV feature, intense at the $\bar{X}$ - point, is recurrent at $\bar{X}'$ but with a significantly reduced amplitude. If this peak corresponds to a surface state [38], one might expect, contrary to observation, that the feature would be enhanced at high emission angles.

IX. METAL - INSULATOR TRANSITION

We have observed that many of the spectral features show relative insensitivity to changes in oxygen stoichiometry throughout the superconducting region of the phase diagram. For example, in Fig. 17 we show EDC's, with hν = 24 eV, scanning the $\bar{\Gamma}$-$\bar{Y}(\bar{X})$ direction for samples with several different stoichiometries. Panels a and b show EDC's for x = 6.9 and x = 6.4, representing both extremes of the superconducting phase field. While differences are apparent in these spectra, prominent features and their dispersive character are very similar. However, with a slight additional reduction of the x = 6.4 sample, such that the sample begins to show semiconducting behavior, profound changes appear in the EDC's (Fig. 17c). Most apparent is the abrupt dramatic attenuation of the 1 eV resonant feature and loss of spectral intensity at the Fermi level. While the residual, underlying band structure also changes more rapidly in the semiconducting region than in the superconducting region, the spectra in panel 17c retain a strong resemblance to the oxygen-rich EDC's. With further oxygen depletion (Fig. 17 d), the 1 eV feature is completely lost. Figure 18 shows an overlay, for x = 6.4, 6.3 and 6.2 samples, of EDC's at the $\bar{Y}(\bar{X})$ point . With increasing oxygen depletion, spectral weight is rapidly lost between 0 - 4 eV binding energy. Especially, the 1 eV feature and the peak near E_F are rapidly lost. A k-space point-by-point comparison of EDC's, with hν = 21.2 eV, for samples with different stoichiometries on both sides of the metal-insulator transition was also presented in ref. 7 for measurements along the zone diagonal. Those measurements, taken near E_F, also showed an abrupt loss of intensity near E_F as the material transformed from a metal to a semiconductor. The significant loss of spectral

weight that occurs in the band near E_F as the insulating gap opens suggests a repopulation of states from this low lying band. This repopulation is apparently associated with the onset of correlation effects that are sufficiently strong to induce a charge transfer gap and a transition to insulating behavior.

Figure 19 shows additional EDC's for x = 6.3 and 6.5 samples, representing both the superconducting and semiconducting regions of the phase field near the M-I transition. These spectra, presenting specific k-point comparisons, were taken along the $\bar{\Gamma}$-$\bar{Y}(\bar{X})$ direction at hν = 28 eV. Generally, these EDC's show a strong point-by-point correspondence, though some modification and relative shifting of spectral features is observed. Like Fig. 18, it is also clear that spectral weight near E_F is substantially reduced as the material becomes semiconducting. (However, the dispersive behavior of the attenuated peak that occurs near E_F remains comparable to that of the superconducting sample [see Fig. 13 and ref. 6]).

A comparison of spectra near E_F, taken with hν = 17 eV, was also made in ref. 6 for samples with x = 6.9 and at 6.35 (metal and insulator). The very sharp feature at E_F was no longer observable as the sample became semiconducting. For YBCO , it appears that loss of spectral weight near E_F with the development of a charge transfer gap [42] and loss of acute resonant features are characteristic changes associated with the transformation from metal to insulator as oxygen is removed.

Changes in ARPES spectra with oxygen stoichiometry are most profound near the metal-insulator transition. Thus we might expect that variations of ARPES spectra with changes in vacancy order will also be most apparent near the metal insulator transition. Assuming that the dependence of ARPES features on vacancy order will mimic the dependence

on oxygen stoichiometry, we expect that, near x = 6.4, resonant ARPES features and spectral weight near E_F will be lost as disorder is added (driving the material insulating). With room temperature annealing, these features will presumably be restored. While such low temperature annealing experiments have not yet been undertaken (they are complicated to perform since samples degrade badly at room temperature), they would provide a useful direct observation of the variation of the occupied electron states that are affected by variations in the state of order.

X. CONCLUSIONS

Using angle resolved photoemission measurements, occupied electron states were extensively studied in the vicinity of the Fermi level for $YBa_2Cu_3O_x$ samples when x was varied to survey both the superconducting and insulating regions of the composition field. For x = 6.9 material, the Fermi surface was measured in detail throughout the Brillouin zone. Measured surfaces, centered at the S-point of the Brillouin zone, closely correspond to (predominately) plane-derived surfaces predicted by band theory. These surfaces appear to be very insensitive to changes in oxygen stoichiometry. Other Fermi surfaces, near the $\bar{\Gamma}$-$\bar{Y}(\bar{X})$ symmetry line, appear to be chain-derived features; these surfaces show greater sensitivity to variations in oxygen content. The small chain-related Fermi surface predicted to occur near the $\bar{S}$-point of the Brillouin zone was not observed at any stoichiometry.

Intense spectral features with resonant character appear in a number of different measurements (specific hν's, and k-points). Particularly sharp and intense features are observed at E_F and at 1 eV

binding energy. These resonant features are severely attenuated as the material transforms from a superconducting metal to an insulator. A dramatic loss of spectral weight also occurs at E_F as the material goes through the metal-insulator transition.

Like variations in oxygen stoichiometry, oxygen vacancy ordering, that occurs in the chain basal plane of oxygen deficient YBCO, exerts a profound effect on both normal state and superconducting properties. Consequently the role of ordering must be carefully examined. No ARPES studies have yet been undertaken to examine the effect of varied order. However, such measurements would appear to be important, providing a direct observation of changes in occupied electron states associated with varied states of order.

ACKNOWLEDGMENTS

The authors gratefully acknowledge Dr. J. J. Yu and Prof. A. J. Freeman for permission to quote results of their calculations for $YBa_2Cu_3O_{6.5}$ prior to publication. Work at Argonne National Laboratory is supported by the U.S. DOE under contract #W-31-109-ENG-38 (BWV,APP,HS,JWD) and by the NSF, Science and Technology Center for Superconductivity, under contract #DMR 8809854 (RL). Ames Laboratory is operated for U.S. DOE by Iowa State University under contract #W-7405-ENG-82. The Synchrotron Radiation Center is supported by NSF under contract #DMR 8601349.

REFERENCES

1. K. Levin, J. H. Kim, J. P. Lu, Q. Si, Physica C **175** (1991) 449; "Physical Properties of High Temperature Superconductors I", edited by Donald M. Ginsberg (World Scientific, Singapore, 1989).
2. P. W. Anderson, Science, **256** (1992) 1526.
3. W. E. Pickett, H. Krakauer, R. E. Cohen and D. J. Singh, Science, **255** (1992) 46.
4. P. Allen, Comments Cond. Mat. Phys., **15** (1992) 327.
5. P. B. Littlewood and C. M. Varma, Phys. Rev B **46** (1992-I) 405.
6. R. Liu, B. W. Veal, A. P. Paulikas, J. W. Downey, P. J. Kostić, S. Fleshler, U. Welp, C. G. Olson, X. Wu, A. J. Arko and J. J. Joyce, Phys. Rev B **46** (1992) (to appear).
7. R. Liu, B. W. Veal, A. P. Paulikas, J. W. Downey, H. Shi, C. G. Olson, C. Gu, A. J. Arko and J. J. Joyce, Phys. Rev. B **45** (1992-II) 5614.
8. R. Liu, B. W. Veal, A. P. Paulikas, J. W. Downey, H. Shi, C. G. Olson, C. Gu, A. J. Arko, J. J. Joyce and R. J. Bartlett, J. Phys. Chem. Solids **52** (1991) 1437.
9. J. C. Campuzano, G. Jennings, M. Faiz, L. Beaulaigue, B. W. Veal, J. Z. Liu, A. P. Paulikas, K. Vandervoort, H. Claus, R. S. List, A. J. Arko, and R. J. Bartlett, Phys. Rev. Lett. **64** (1990) 2308; J. C. Campuzano, L. C. Smedskjaer, R. Benedek, G. Jennings and A. Bansil, Phys. Rev. B **43** (1991) 2788.

10. J. G. Tobin, C. G. Olson, C. Gu, J. Z. Liu, F. R. Solal, M. J. Fluss, R. H. Howell, J. C. O'Brien, H. B. Radousky, and P. A. Sterne, Phys. Rev. B **45** (1992).

11. G. Mante, R. Claessen, A. Huss, R. Manzke, and M. Skibowski, Th. Wolf, M. Knupfer, and J. Fink, Phys. Rev. B **44** (1991-I) 9500.

12. G. Mante, R. Claessen, T. Buslaps, S. Harm, R. Manzke, M. Skibowski, and J. Fink, Z. Phys. B **80** (1990) 181.

13. L. C. Smedskjaer, J. Z. Liu, R. Benedek, D. G. Legnini, D. J. Lam, M. D. Stahulak, H. Claus and A. Bansil, Physica C **156** (1988) 269; L. C. Smedskjaer, A. Bansil, U. Welp, Y. Fang and K. G. Bailey, Physica C **192** (1992) 259.

14. H. Haghighi, J. H. Kaiser, S. Rayner, R. N. West, J. Z. Liu, R. Shelton, R. Howell, F. Solal, and M. J. Fluss, Phys. Rev. Lett. **67** (1991) 382.

15. F. M. Mueller, C. M. Fowler, B. L. Freeman, W. L. Hults, J. C. King, J. L. Smith, Physica B **172** (1991) 253.

16. G. Kido, K. Komorita, H. Katayama-Yoshida, T. Takahashi, J. of Phys. and Chem. of Solids **52** (1991) 1465.

17. F. Herman, R. V. Kasowski, and W. Y. Hsu, Phys. Rev. B **36** (1987) 6904.

18. M. Hirao, T. Uda and Y. Murayama, Physica C **195** (1992) 230.

19. B. X. Yang, J. M. Tranquada and G. Shirane, Phys. Rev. B **38** (1988) 174.

20. R. Beyers and T. M. Shaw, in: Solid State Physics, Advances in Reaearch and Applications, eds. H. Ehrenreich and D. Turnbull (Academic, New York, 1989) p. 135.

21. B. W. Veal, A. P. Paulikas, H. You, H. Shi, Y. Fang and J. W. Downey, Phys. Rev. B **42** (1990) 6305; J. D. Jorgensen, S. Pei, P. Lightfoot, H. Shi, A. P. Paulikas and B. W. Veal, Physica C 167 (1990) 571.

22. J. D. Jorgensen, B. W. Veal, A. P. Paulikas, L. W. Nowicki, G. W. Crabtree, H. Claus and W. K. Kwok, Phys. Rev. B **41** (1990) 1863.

23. A. J. Arko, R. S. List, R. J. Bartlett, S.-W. Cheong, Z. Fisk, J. D. Thompson, C. G. Olson, A.-B. Yang, R. Liu, C. Gu, B. W. Veal, J. Z. Liu, A. P. Paulikas, K. Vandervoort, H. Claus, J. C. Campuzano, J. E. Schirber and N. D. Shinn, Phys. Rev. B **40** (1989) 2268.

24. H. W. Zandbergen, Physica C **194** (1992) 287.

25. The phase boundary depends on temperature, oxygen pressure and order in the chain basal plane. Structural measurements on well annealed (but metastable) samples at ambient conditions show that the phase boundary occurs near x = 6.4 [21].

26. K. Matsuishi, Y.-K. Tao, H.-S. Feng, P.-H. Hor and C.-W. Chu, Physica C **185-189** (1991) 827.

27. J. Kircher, E. Brücher, E. Schönherr, R. K. Kremer and M. Cardona, Phys. Rev. B **46** (1992-I) 588.

28. I. N. Kuropyatnik and A. N. Lavrov, Physica C **197** (1992) 47.

29. Unpublished.

30. R. McCormack, D. deFontaine and G. Ceder, Phys. Rev. B **45** (1992) 12976.

31. R. Gupta and M. Gupta, Phys. Rev B **44** (1991-II) 2739.

32. B. W. Veal and A. P. Paulikas, Physica C **184** (1991) 321.

33. S. Massidda, J. Yu, K. T. Park and A. J. Freeman, Physica C **176** (1991) 159. The band structure in Fig. 5 incorporates improved sampling of the Brillouin zone relative to earlier results: J. Yu, S. Massidda, A. J. Freeman and D. D. Koelling, Phys. Lett. A **122** (1987) 203; A. J. Freeman, J. Yu, S. Massidda, D. D. Koelling, Physica B **148** (1987) 212. Further, the recent calculation does not make the assumption of chain-plain decoupling in the Γ-Y region as was done in the earlier Fermi surface analysis.

34. W. E. Pickett, Rev. Mod. Phys. **61** (1989) 433; W. E. Pickett, R. E. Cohen, and H. Krakauer, Phys. Rev. B **42** (1990) 8764; H. Krakauer, W. E. Pickett, and R. E. Cohen, J. of Superconductivity **1** (1988) 111.

35. O. K. Andersen, A. I. Liechtenstein, O. P[illegible]riquez, I. I. Mazin, O. Jepsen, V. P. Antropov, O. Gunnarsson and S. Gopalan, Physica C **185-189** (1991) 147; I. I. Mazin, O. Jepsen, O. K. Andersen, A. I. Liechtenstein, S. N. Rashkeev and Y. A. Uspenskii, Phys. Rev. B **45** (1992-I) 5103.

36. J. Yu and A. J. Freeman, private communication.

37. C. G. Olson, R. Liu, D. W. Lynch, R. S. List, A. J. Arko, B. W. Veal, Y. C. Chang, P. Z. Jiang, and A. P. Paulikas, Phys. Rev. B **42** (1990) 381.

38. R. Claessen, G. Mante, A. Huss, R. Manzke, M. Skibowski, Th. Wolf and J. Fink, Phys. Rev. B **44** (1991-I) 2399; R. Manzke, G. Mante, M. Skibowski, and J. Fink, Physica C **185-189** (1991) 843.

39. Recent data indicate that the measured E_F in Fig. 13 might be slightly shifted (to positive binding energy) suggesting that the dispersing peak approaches E_F without crossing.

40. C. G. Olson, C. Gu, X. Wu, D. W. Lynch, J. G. Tobin, G. D. Waddill, M. J. Fluss and J. Z. Liu, Bull. Am. Phys. Soc. 37 (1992) 120.

41. The 1 eV feature shown in Fig. 14b was somewhat attenuated relative to results from a freshly cleaved surface. See ref. 8.

42. S. L. Cooper, D. Reznik, A. Kotz, M. A. Karlow, R. Liu, M. V. Klein, W. C. Lee, J. Giapintzakis, D. M. Ginsberg, B. W. Veal, and A. P. Paulikas, to be published.

FIGURE CAPTIONS

Fig. 1. Superconducting transition temperature vs oxygen stoichiometry for $YBa_2Cu_3O_x$.

Fig. 2. The structure (two unit cells) of $YBa_2Cu_3O_x$ showing plane and chain layers.

Fig. 3. Resistivity measurements for a sample of $YBa_2Cu_3O_{6.41}$ showing the effects of room temperature annealing. The upper curve was measured when the chain layer was "disordered"; i.e., immediately after a quench from 180°C. With aging at room temperature, the sample becomes superconducting and T_c systematically rises to ~20 K. Aging times from top to bottom are (1) as quenched, (2) 43 min, (3) 73 min, (4) 248 min, (5) 493 min, (6) 1003 min, (7) 1983 min, (8) 7743 min. These results are apparently a manifestation of hole doping that is controlled by the state of oxygen vacancy order in the chain basal plane.

Fig. 4. A representation of the chain basal plane in the Ortho II structure of $YBa_2Cu_3O_{6.5}$. (Large dots represent oxygen atoms, small dots represent copper atoms.) The ideal structure contains alternating occupied and vacant (oxygen-free) chains. Cu's in filled chains are 4-coordinated, Cu's in empty chains are 2-coordinated. With elevated temperature, oxygens from normally filled chains move to normally empty chains changing the concentration of 2-coordinated (monovalent) Cu's with consequent change in the hole doping.

Fig. 5. The band structure of $YBa_2Cu_3O_7$ [33].

Fig. 6. (a) The Brillouin zone for $YBa_2Cu_3O_7$. (b) An overlay of Fermi surfaces calculated [33] at $k_z = 0$ (in the plane containing Γ) and at $k_z = \pi/c$ (in the plane containing Z). The shaded regions connect surfaces from common bands that appear in the two planes. The surfaces labeled 1 and 4 have a substantial admix of chain band character. (c) Fermi surfaces calculated by [34] displayed in the same way as panel (b).

Fig. 7. (a) Energy distribution curves (EDC's) for $YBa_2Cu_3O_{6.9}$ taken using hν = 21.2 eV for k-points along $\bar{\Gamma}$-$\bar{S}$, the Brillouin zone diagonal. Photoelectron emission angles relative to the surface normal (θ and φ) are marked next to each curve. A spectral feature appears near 0.3 eV when $\theta = \phi = 4^o$ that disperses to E_F and crosses near $\theta = \phi = 9^o$. A second, poorly defined feature may appear as a shoulder on the low binding energy side (arrow). (b) a series of EDC's from $Bi_2Sr_2CaCu_2O_8$ [37] showing a spectral peak dispersing toward E_F. Note that no shoulder appears in the EDC as the feature approaches E_F.

Fig. 8. Comparison of the measured Fermi surfaces of $YBa_2Cu_3O_{6.9}$ determined from EDC measurements using hν = 21.2 eV and the calculated Fermi surfaces of $YBa_2Cu_3O_7$ (shaded regions) from ref. 34. Data were taken on twinned crystals. The solid circles are determined with greatest clarity.

Fig. 9. Comparison of EDC's (a) for $YBa_2Cu_3O_{6.9}$ along $\bar{\Gamma}$-$\bar{S}$, i.e., with $\theta = \phi$ and (b) for $YBa_2Cu_3O_{6.5}$, again with $\theta = \phi$. Photoelectron emission angles relative to the surface normal (θ and ϕ) are marked next to each curve. All corresponding k-points for EDC's in panel (b) are marked as solid dots in the Brillouin zone for $YBa_2Cu_3O_7$. Note that the spectra in panels (a) and (b) are very similar, including the indicated Fermi level crossing near $\theta = \phi = 9°$.

Fig. 10. Comparison of EDC's along $\bar{\Gamma}$-$\bar{Y}(\bar{X})$ for (a) $YBa_2Cu_3O_{6.9}$ and (b) $YBa_2Cu_3O_{6.5}$. Photoelectron emission angles relative to the surface normal (θ and ϕ) are marked next to each curve. Corresponding k-points for EDC's in panel (a) are marked as solid dots in the $YBa_2Cu_3O_7$ Brillouin zone. Note the difference in EDC's for the two stoichiometries at comparable electron emission angles.

Fig. 11. The calculated Fermi surface for the double cell (Ortho II) structure for the $YBa_2Cu_3O_{6.5}$ composition [36]. Plane band surfaces 2 and 3 remain relatively unchanged from $YBa_2Cu_3O_7$ (Fig. 6).

Fig. 12. EDC's measured on an untwinned $YBa_2Cu_3O_{6.5}$ sample ($T_c = 53$ K), for k-points near $\bar{Y}$, using $h\nu = 17$ eV. An intense, very sharp and nondispersive peak appears near E_F. It is nearly identical to the corresponding feature observed in $YBa_2Cu_3O_{6.9}$ [10].

Fig. 13. EDC's measured on an untwinned $YBa_2Cu_3O_{6.5}$ sample, for k-points along the $\bar{\Gamma}$-$\bar{Y}$-$\bar{\Gamma}'$ line, using $h\nu$ = 28 eV. This dispersive feature is most intense at the $\bar{Y}$-point where it appears very close to E_F.

Fig. 14. EDC's measured on twinned samples of $YBa_2Cu_3O_{6.9}$ using (a) $h\nu$ = 24 eV and (b) $h\nu$ = 74 eV photons. In both panels, a sharp and intense dispersive feature is observed at 1 eV binding energy at the X(Y) points of the Brillouin zone. In panel (a), an intense, though somewhat broader peak is also observed near 1.5 eV at $\bar{\Gamma}$. EDC's are identified by dots in the Brillouin zone section.

Fig. 15. EDC's measured on twinned samples of $YBa_2Cu_3O_{6.9}$ using $h\nu$ = 74 eV. The measurements scan through several Brillouin zones. Strong zone dependent intensity modulations of the spectra near E_F are apparent.

Fig. 16. An amplified presentation of the EDC, shown in Fig. 15, for $k_{||} = 3.67\ A^{-1}$ showing the sharp and intense feature near E_F.

Fig. 17. EDC's measured on samples of $YBa_2Cu_3O_x$ with the oxygen stoichiometries (a) x = 6.9, (b) x= 6.4, (c) x = 6.3 and (d) x = 6.2. Measurements were taken along the $\bar{\Gamma}$-$\bar{Y}(\bar{X})$ symmetry lines using $h\nu$ = 24 eV. Samples (a) and (b) are superconducting, samples (c) and (d) are semiconducting. Note that corresponding EDC's in the superconducting region are very similar but abrupt spectral changes occur when the samples become semiconducting.

Fig. 18. An overlay of EDC's at the $\bar{X}(\bar{Y})$ point for samples with stoichiometries x = 6.4 (superconducting), x = 6.3 and x = 6.2 (both semiconducting) taken with hν = 24 eV. Note that, as samples become semiconducting, a dramatic loss of intensity occurs from states near E_F and from the 1 eV resonant peak.

Fig. 19. An overlay of EDC's for x = 6.5 (superconducting) and x = 6.3 (semiconducting) samples using hν = 28 eV for several points along $\bar{\Gamma}$-$\bar{Y}(\bar{X})$. Again, strong attenuation of the peak near E_F is observed as the sample becomes semiconducting.

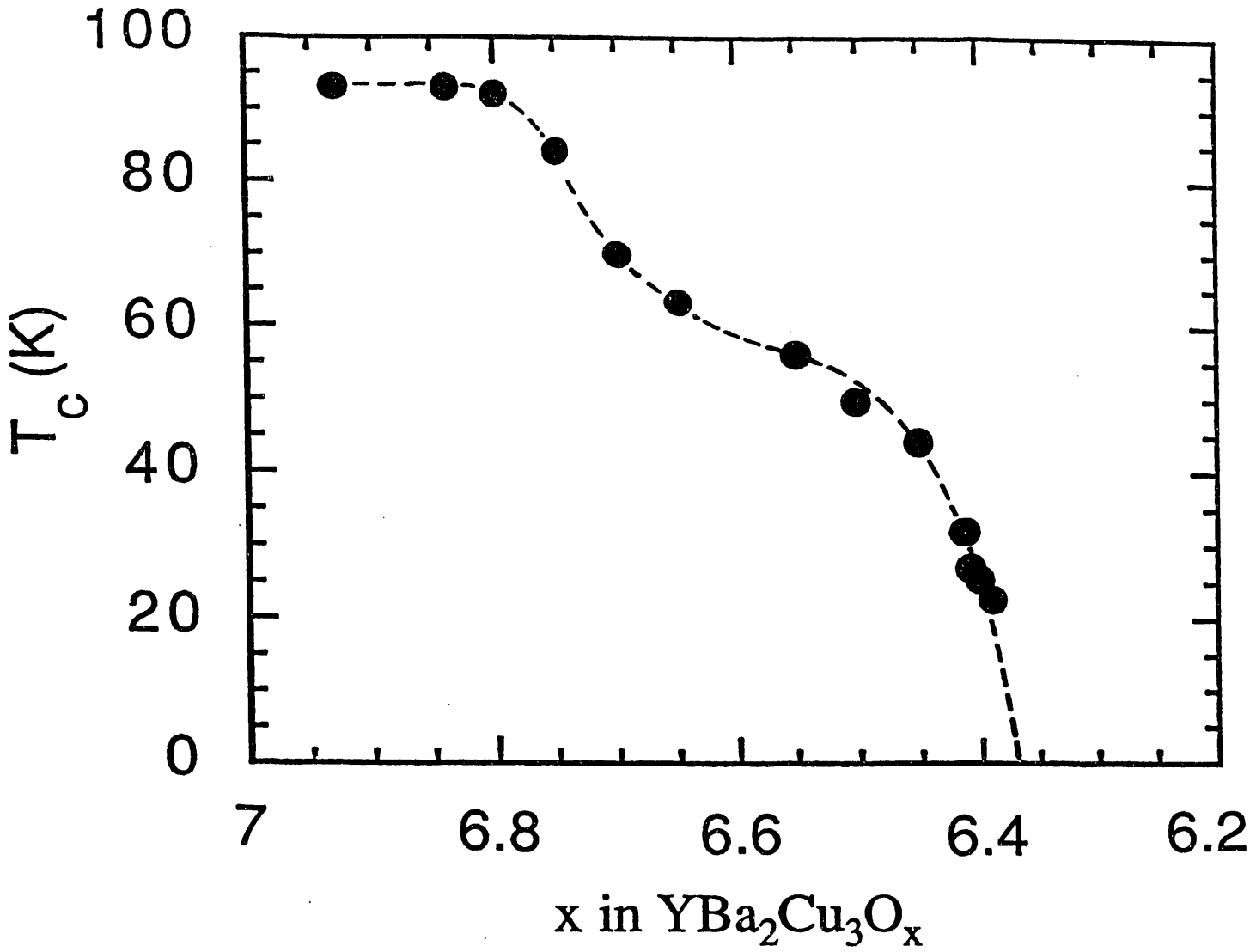
100
80
60
40
20
0
T_c (K)
7
6.8
6.6
6.4
6.2
x in $YBa_2Cu_3O_x$

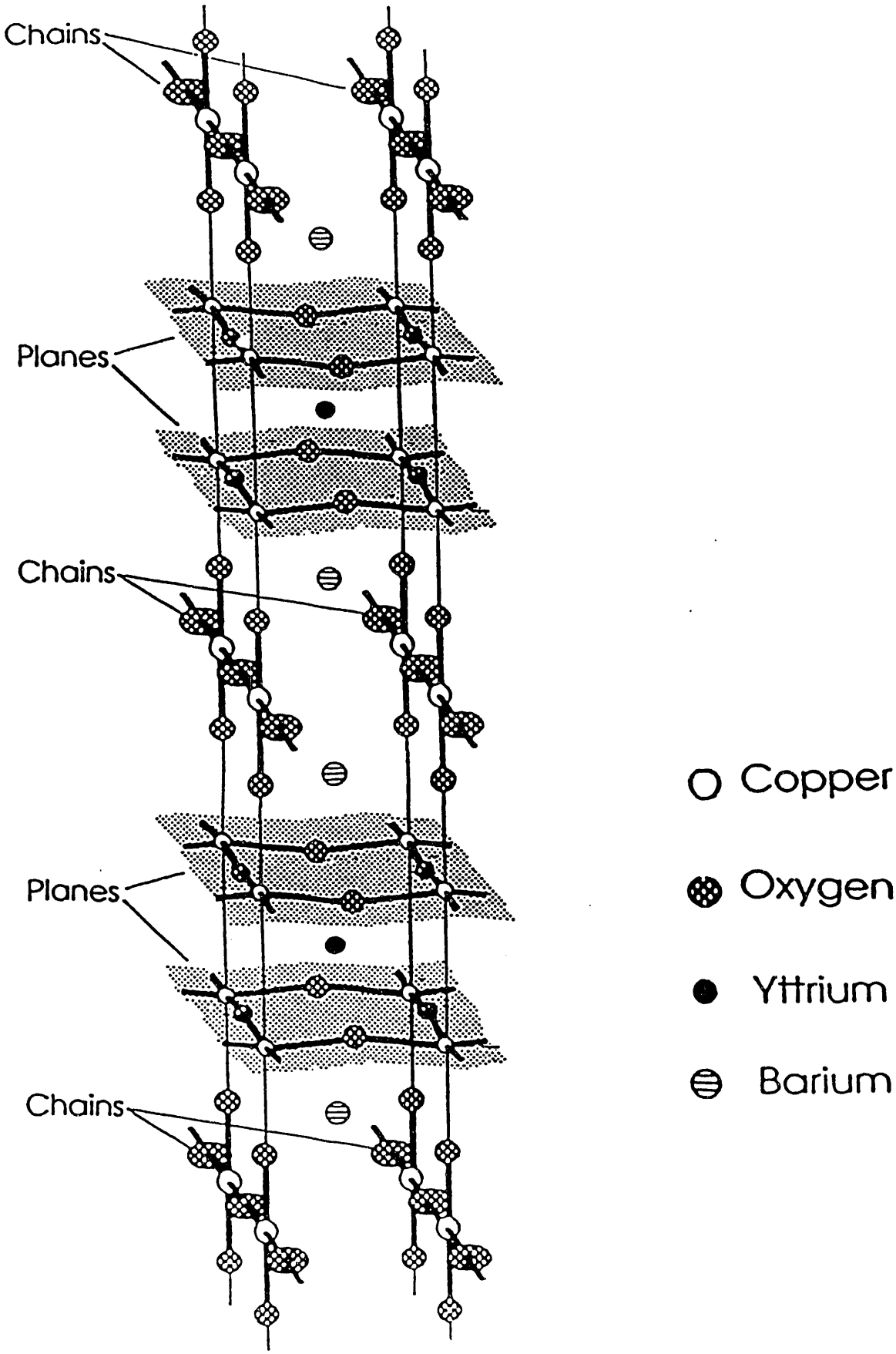
Chains
Planes
Chains
Planes
Chains
Copper
Oxygen
Yttrium
Barium

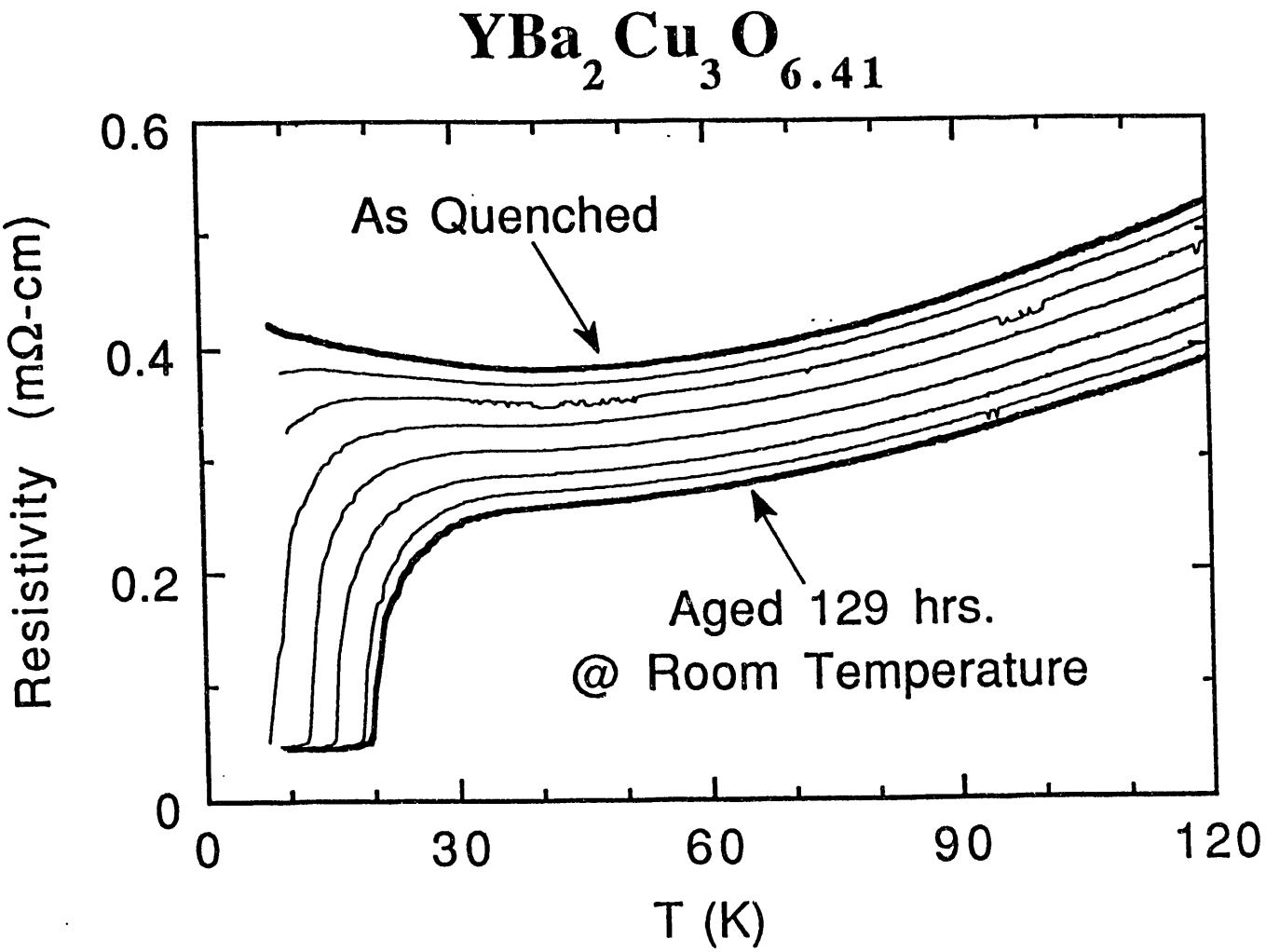
YBa2Cu3O6.41
Resistivity (mΩ-cm)
0.6
0.4
0.2
0
As Quenched
Aged 129 hrs.
@ Room Temperature
0
30
60
90
120
T (K)

$YBa_2Cu_3O_{6.5}$

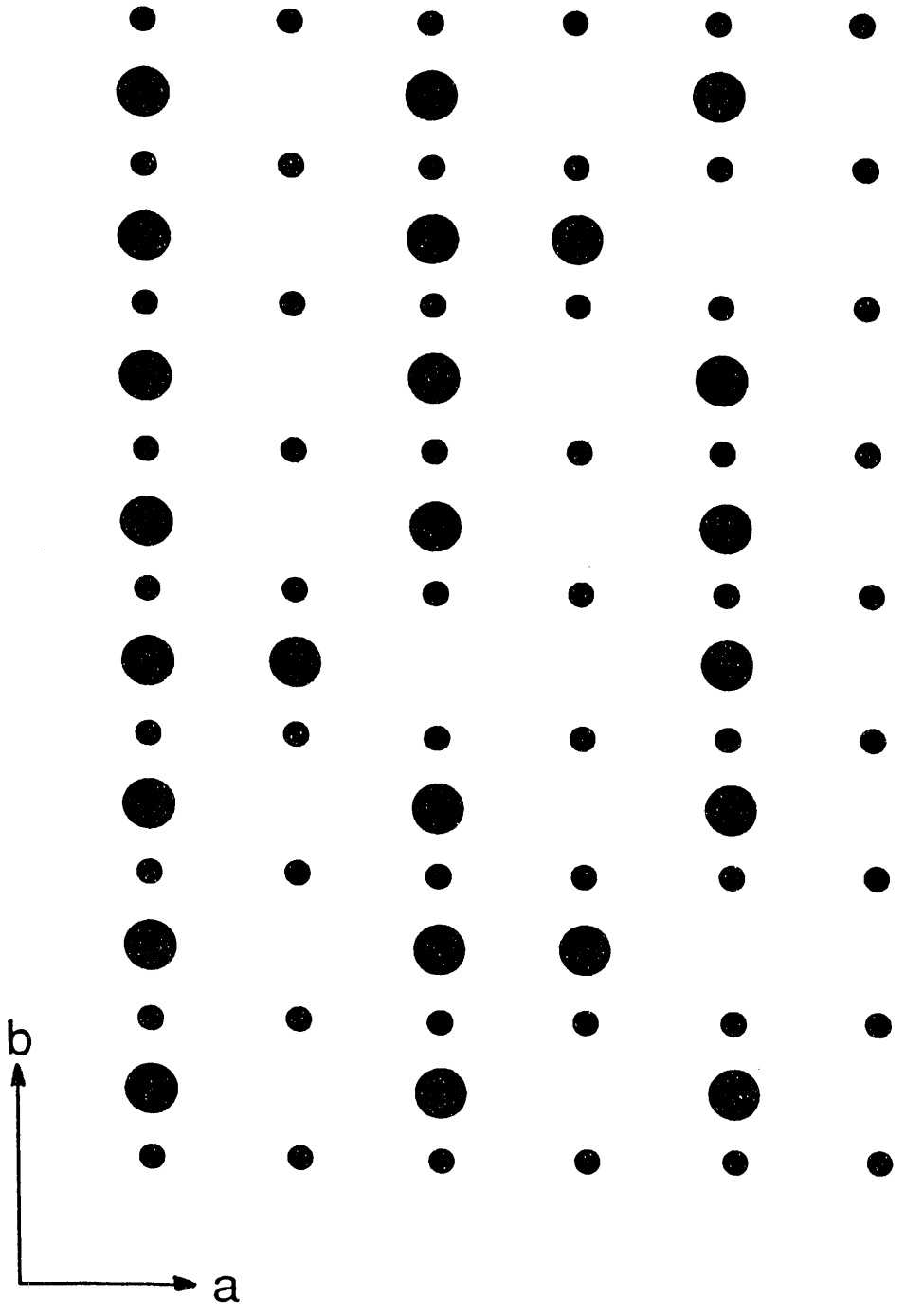

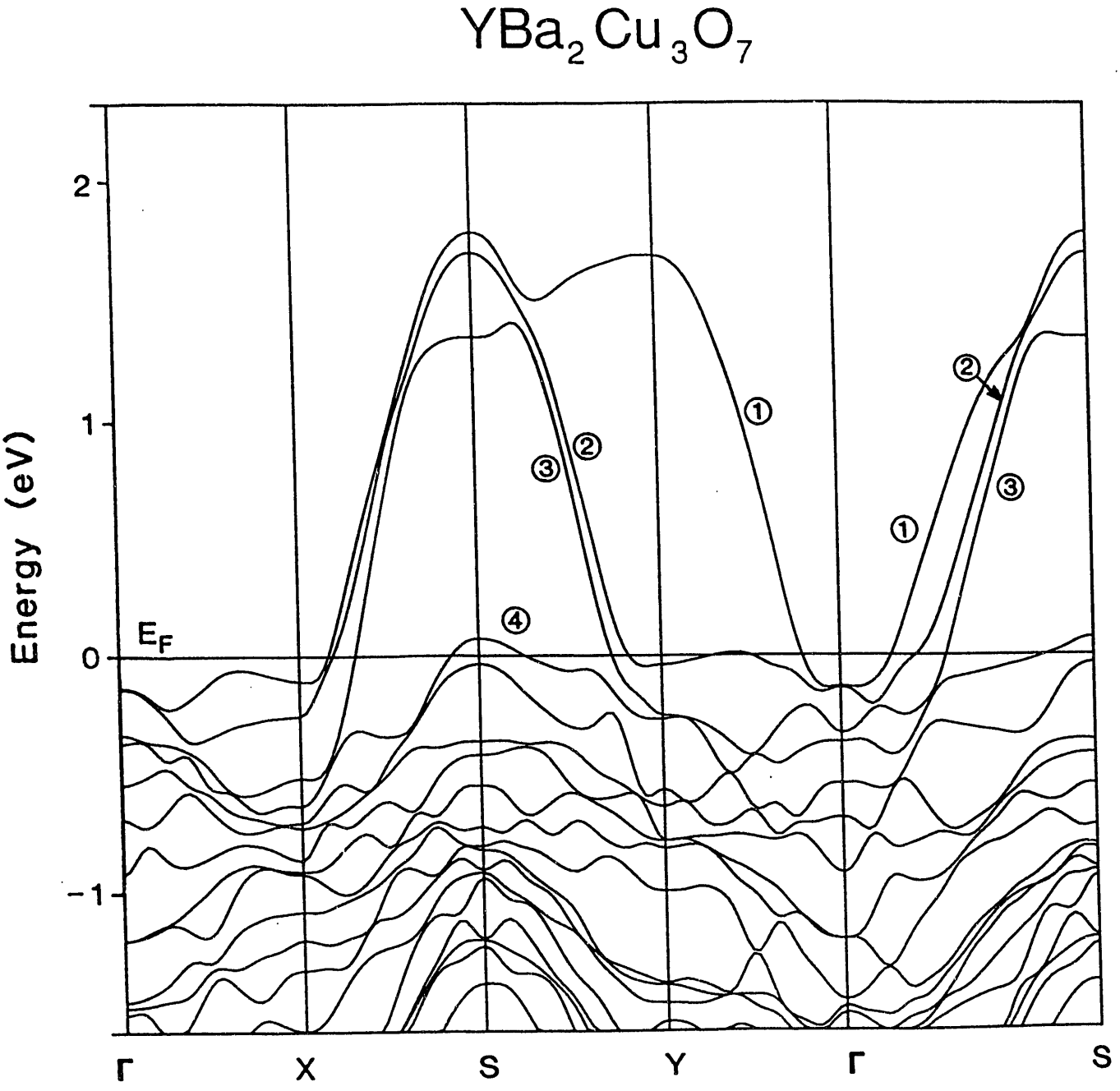
YBa2Cu3O7
Energy (eV)
2
1
0
−1
EF
①
②
③
④
Γ
X
S
Y
Γ
S

(a)

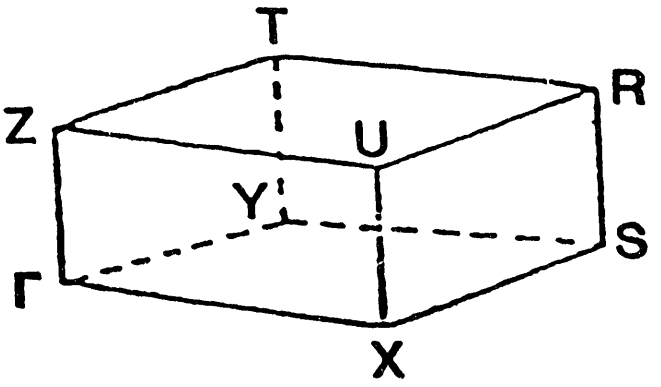

(b)

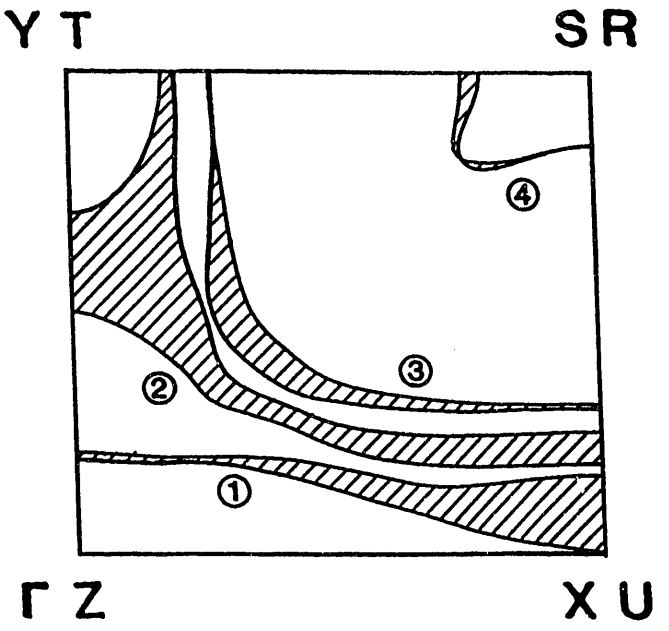

(c)

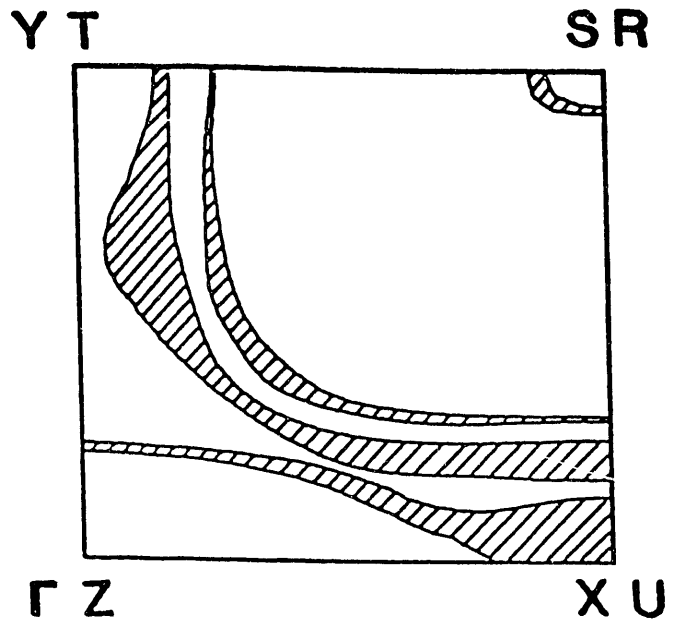

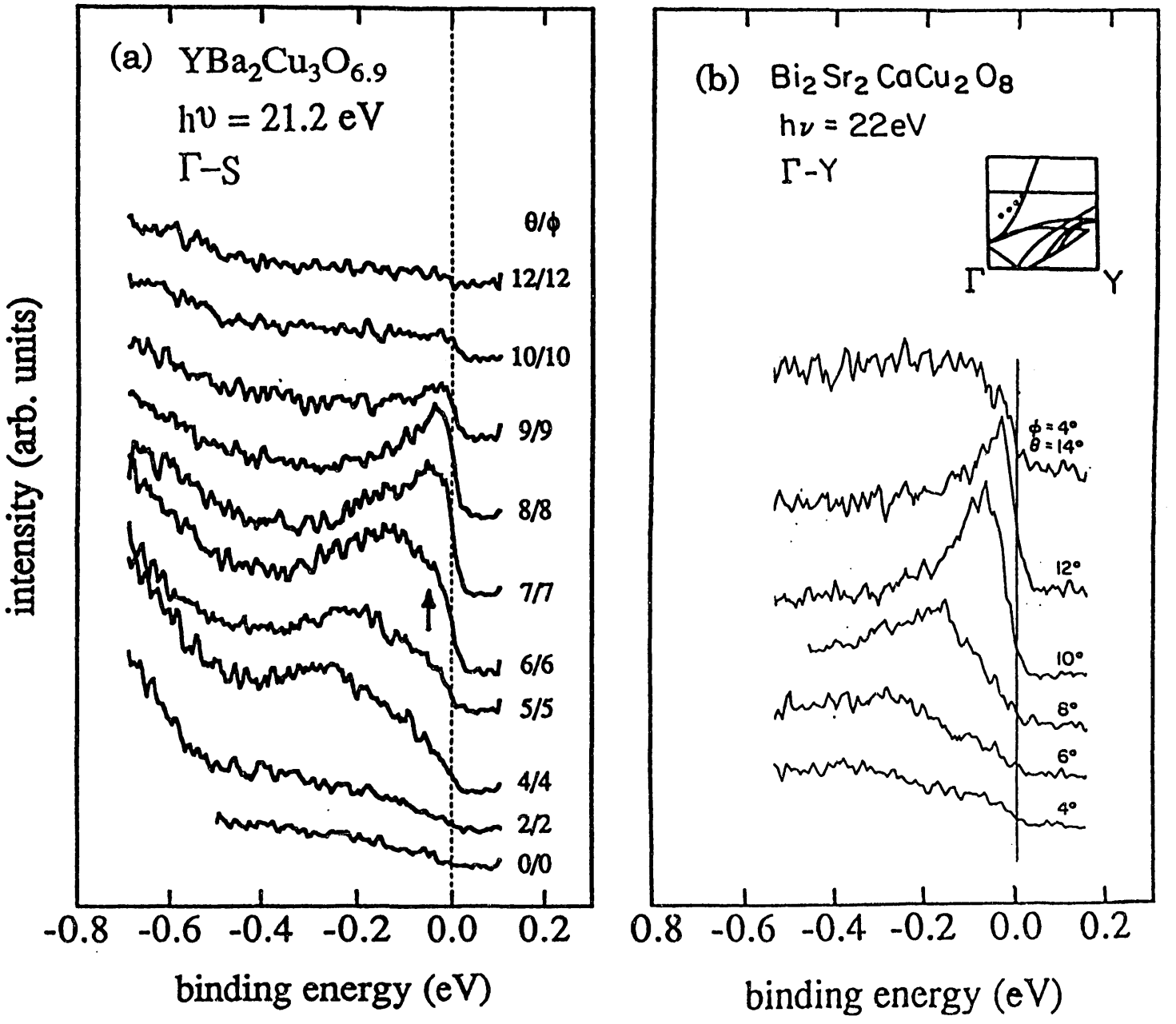
(a) $YBa_2Cu_3O_{6.9}$
hυ = 21.2 eV
Γ–S
θ/ϕ
12/12
10/10
9/9
8/8
7/7
6/6
5/5
4/4
2/2
0/0
intensity (arb. units)
-0.8 -0.6 -0.4 -0.2 0.0 0.2
binding energy (eV)
(b) $Bi_2Sr_2CaCu_2O_8$
hν = 22eV
Γ-Y
Γ
Y
ϕ = 4°
θ = 14°
12°
10°
8°
6°
4°
0.8 -0.6 -0.4 -0.2 0.0 0.2
binding energy (eV)

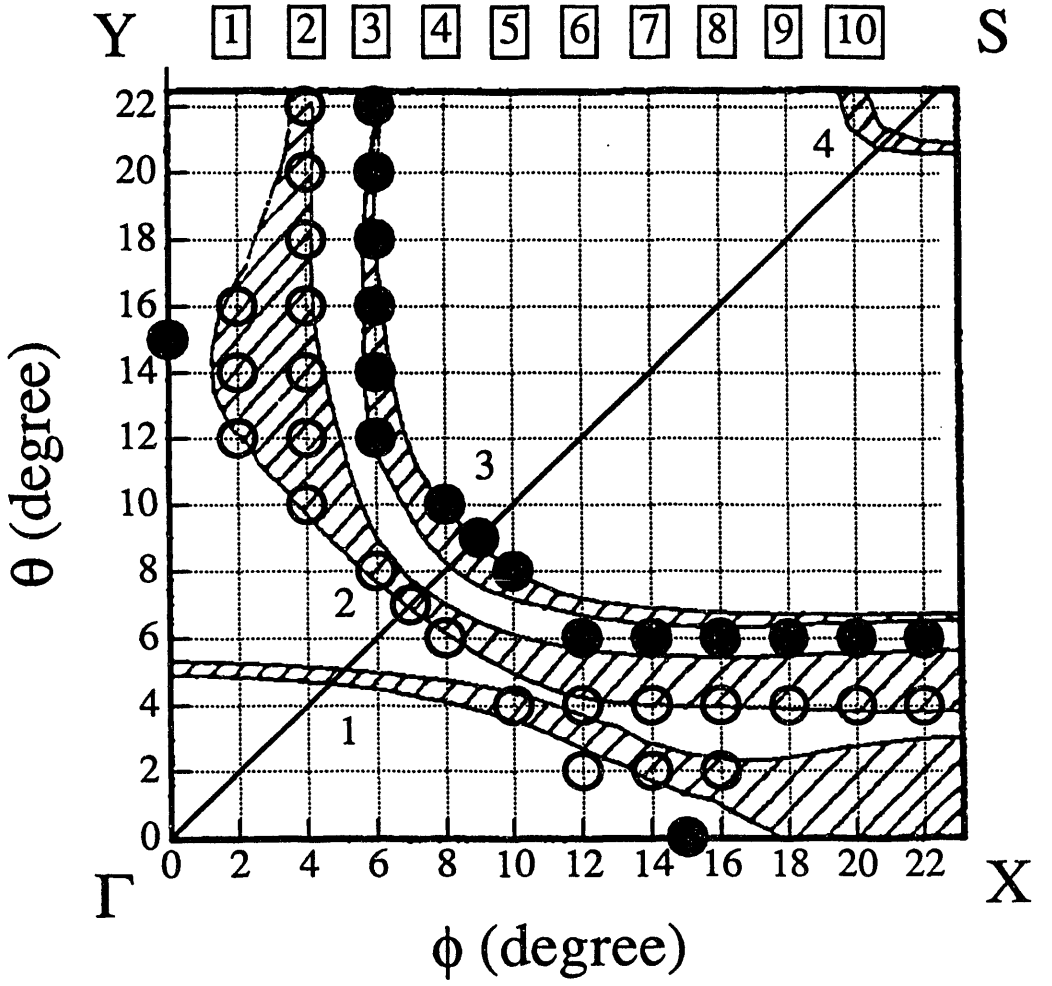
Y
1
2
3
4
5
6
7
8
9
10
S
θ (degree)
22
20
18
16
14
12
10
8
6
4
2
0
0
2
4
6
8
10
12
14
16
18
20
22
Γ
X
ϕ (degree)
1
2
3
4

$YBa_2Cu_3O_x$

$h\upsilon = 21.2$ eV

Γ–S

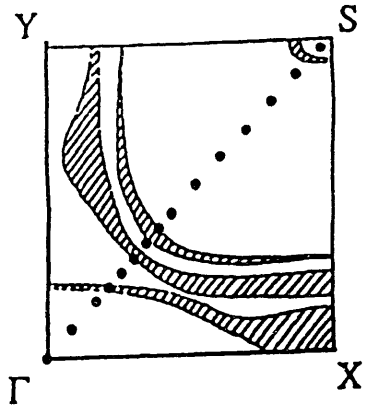

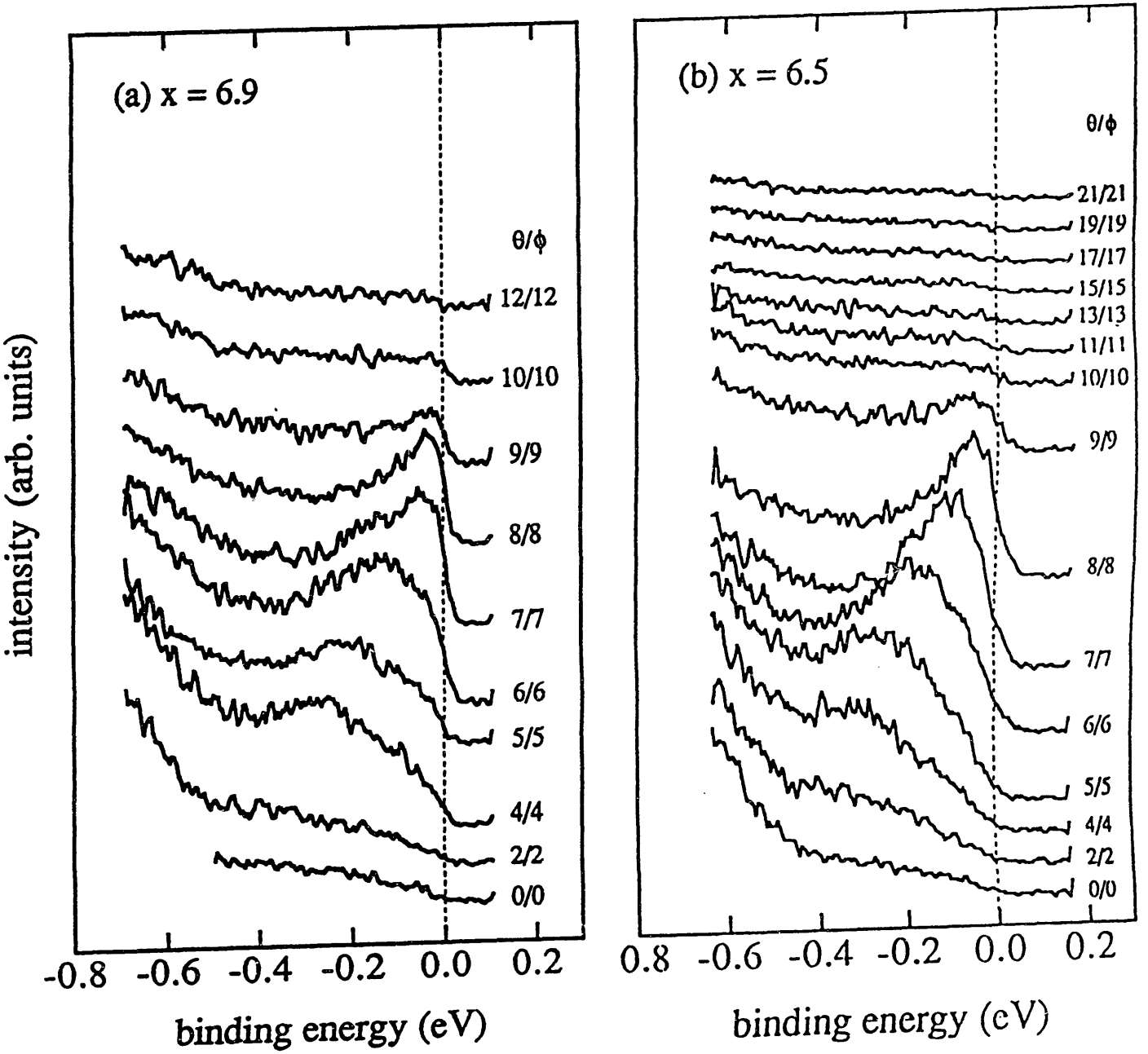

$YBa_2Cu_3O_x$

$h\upsilon = 21.2$ eV

Γ–Y(X)

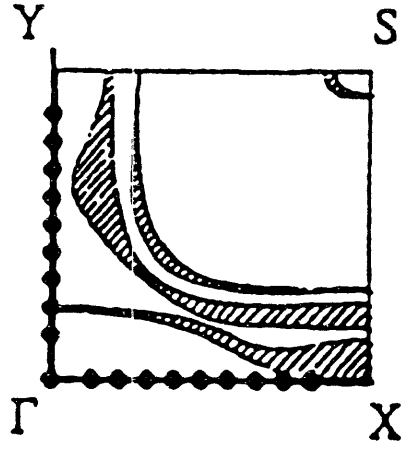

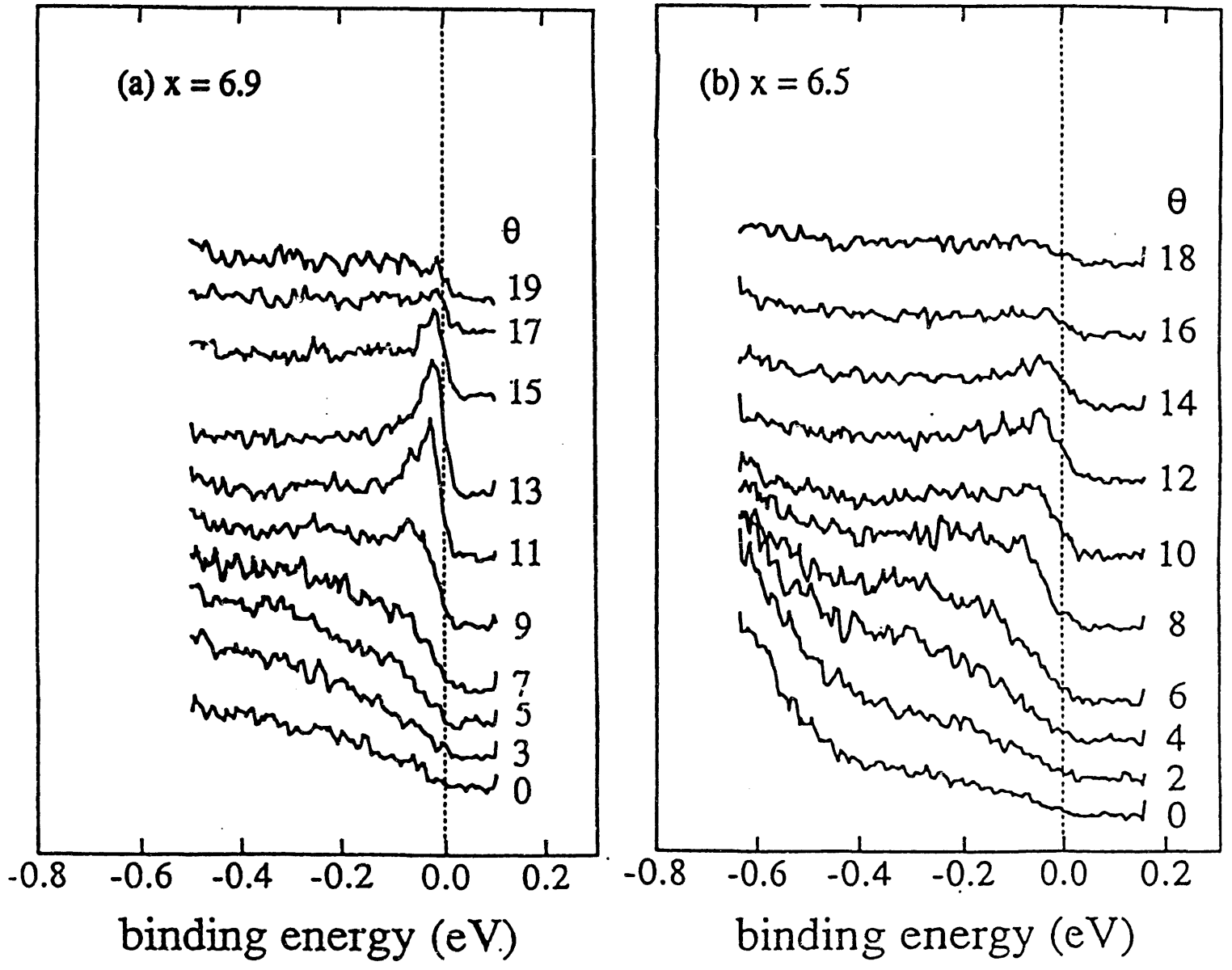

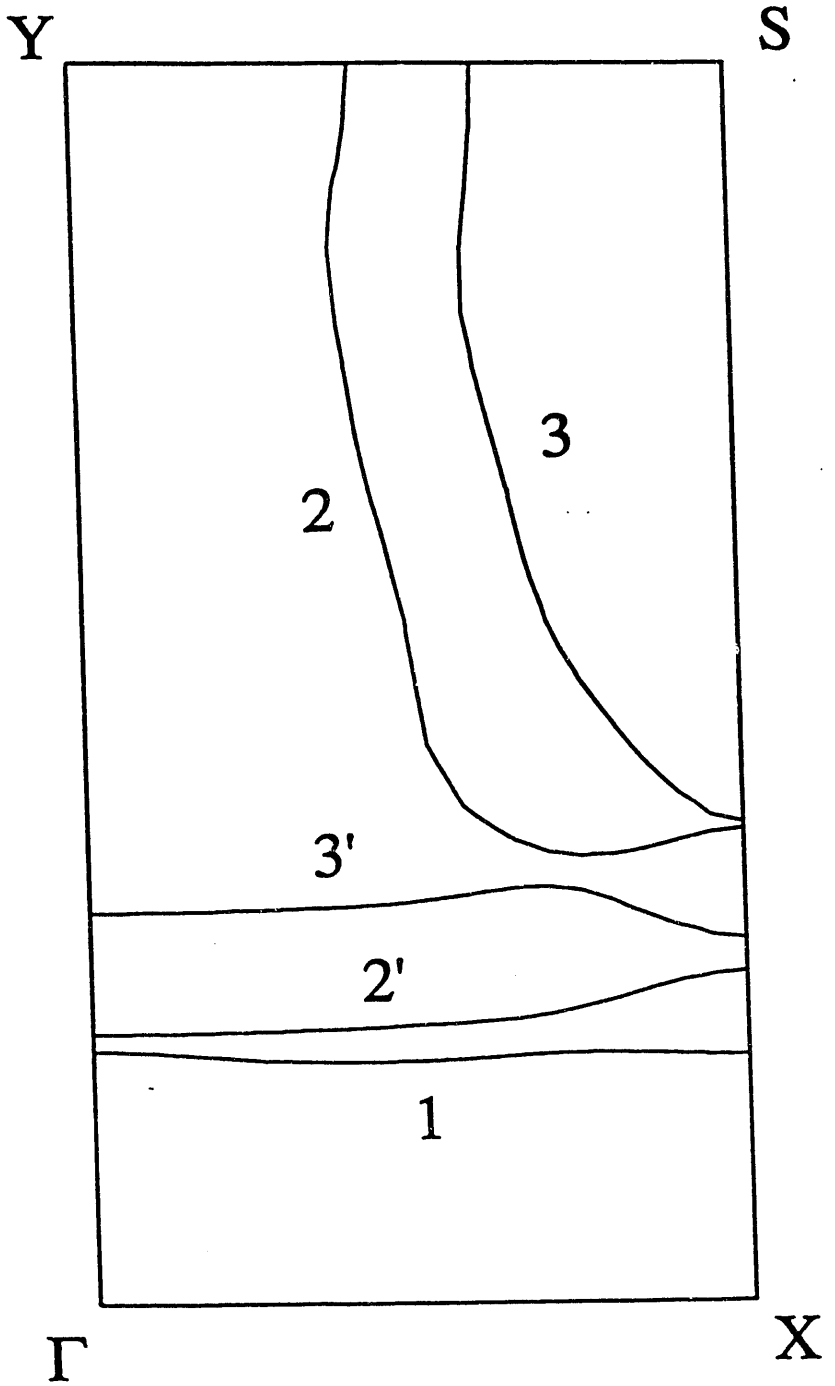
Y
S
3
2
3'
2'
1
Γ
X

$YBa_2Cu_3O_{6.5}$
(untwinned)
$h\upsilon = 17$ eV

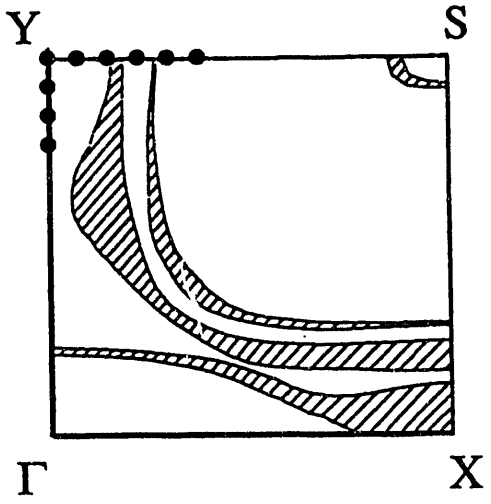

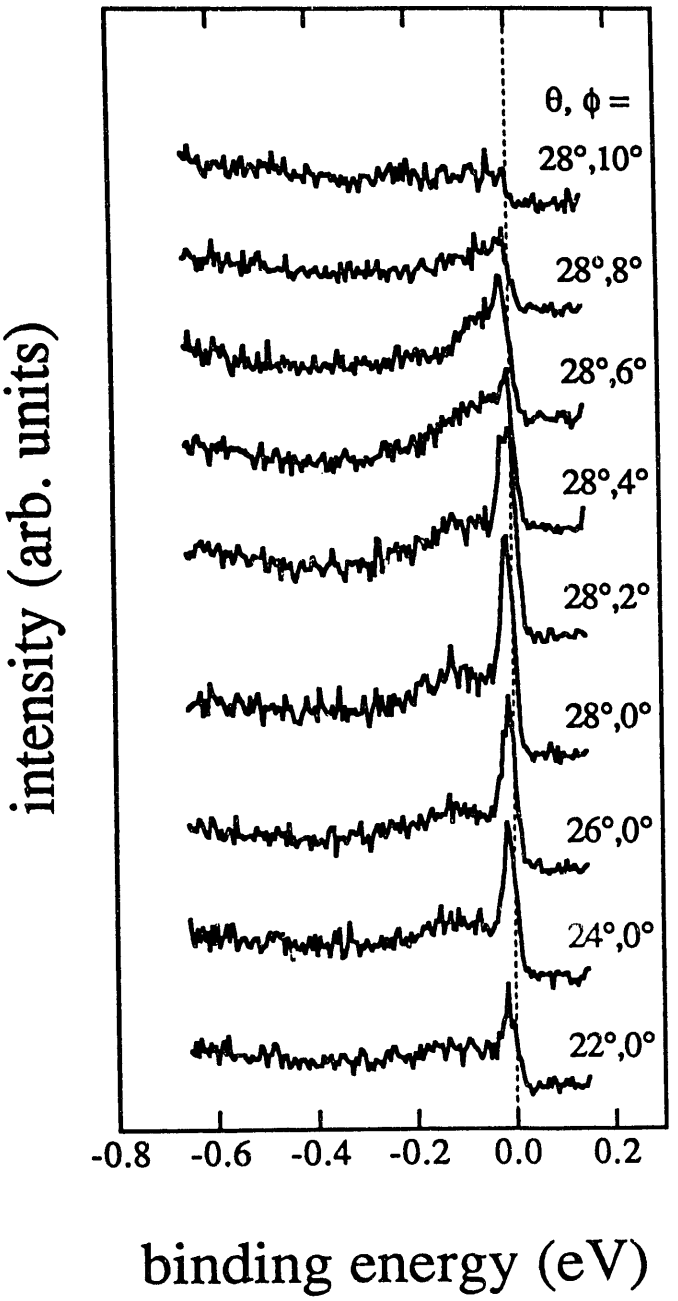

$YBa_2Cu_3O_{6.5}$
(untwinned)
$h\upsilon = 28$ eV

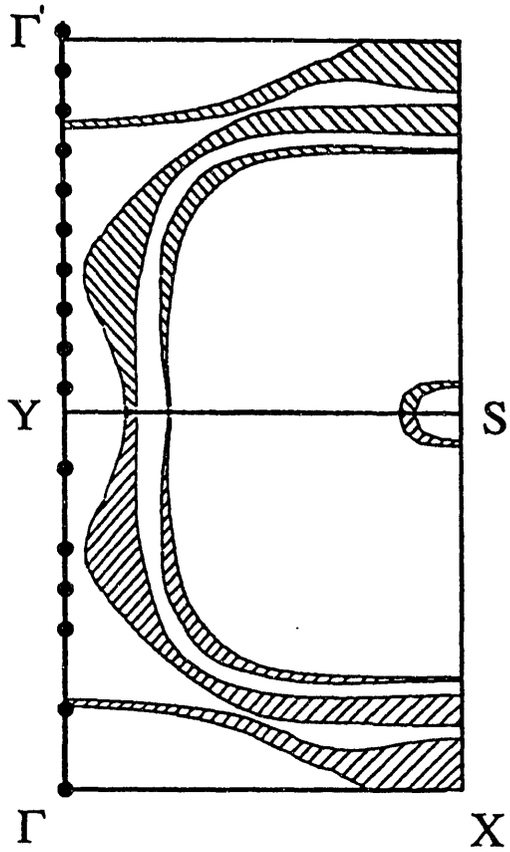

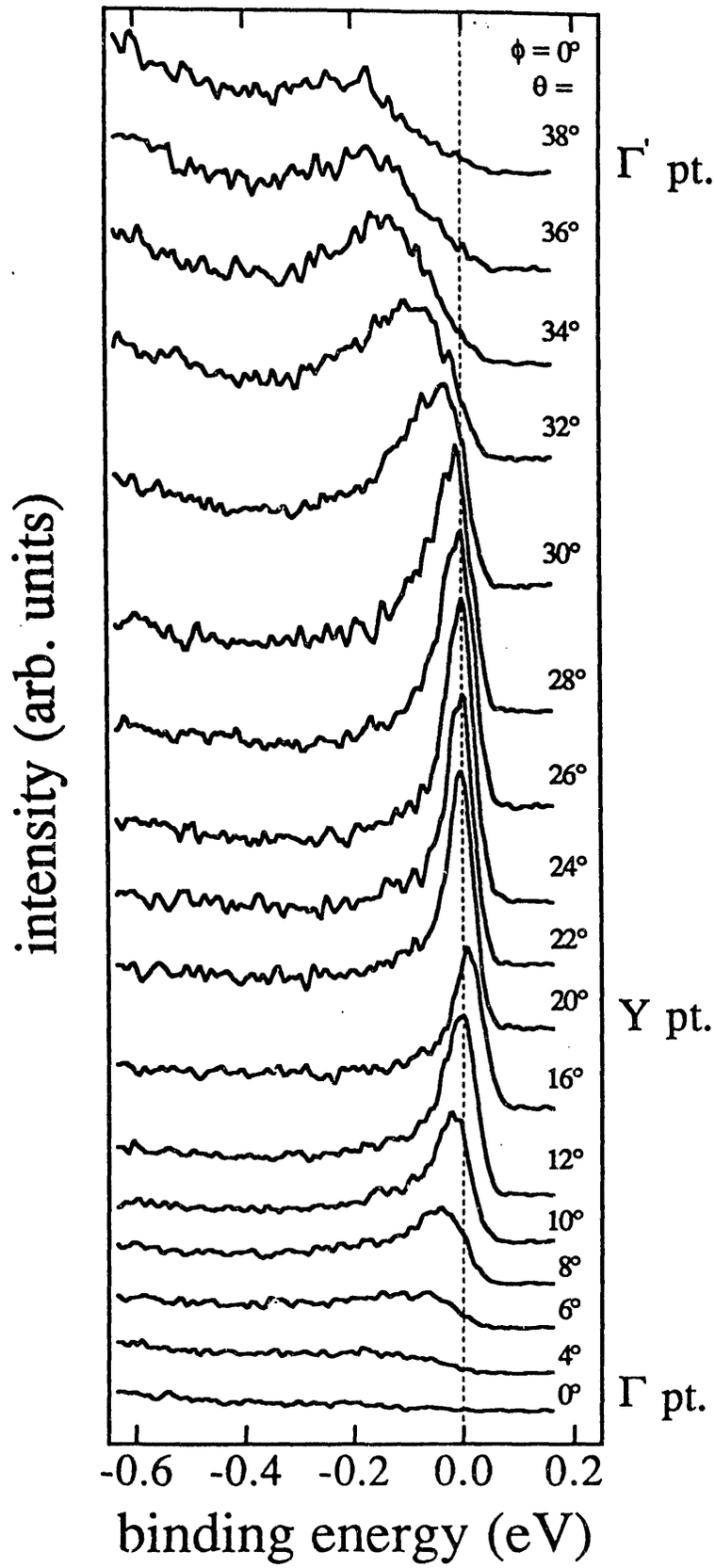

$YBa_2Cu_3O_{6.9}$, Γ - X(Y)

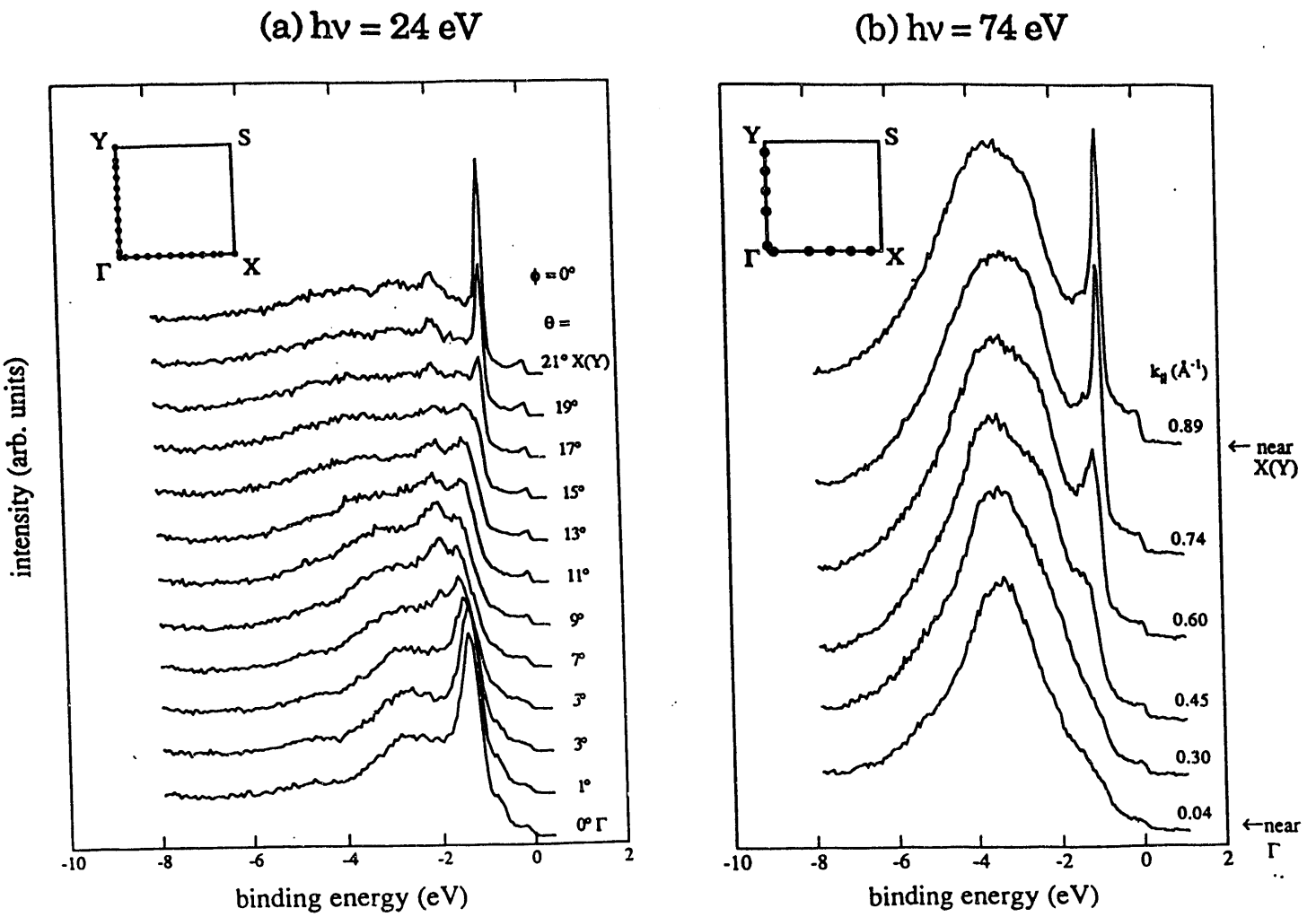

$YBa_2Cu_3O_{6.9}$

$h\upsilon = 74$ eV

Normalized to beam current

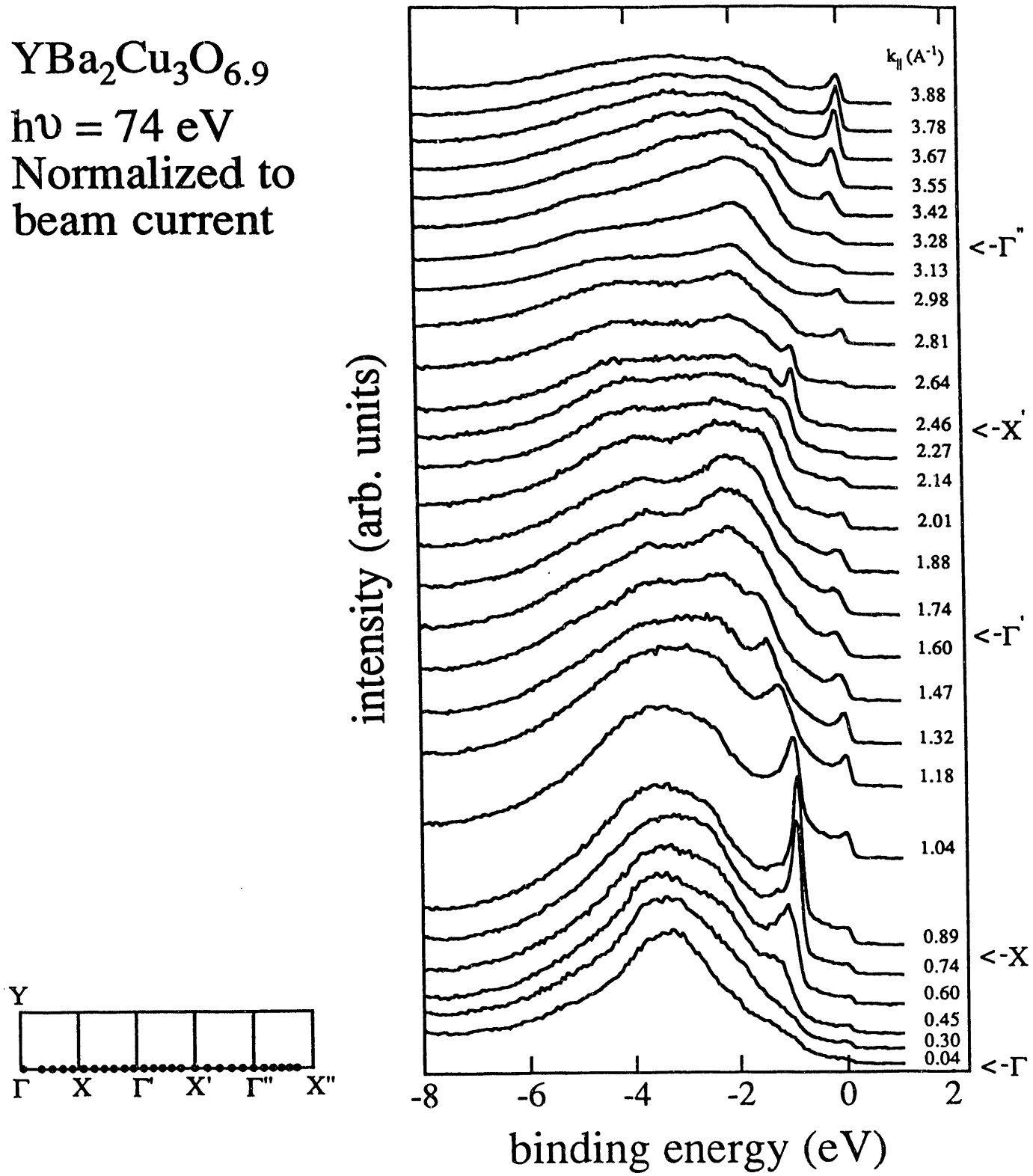

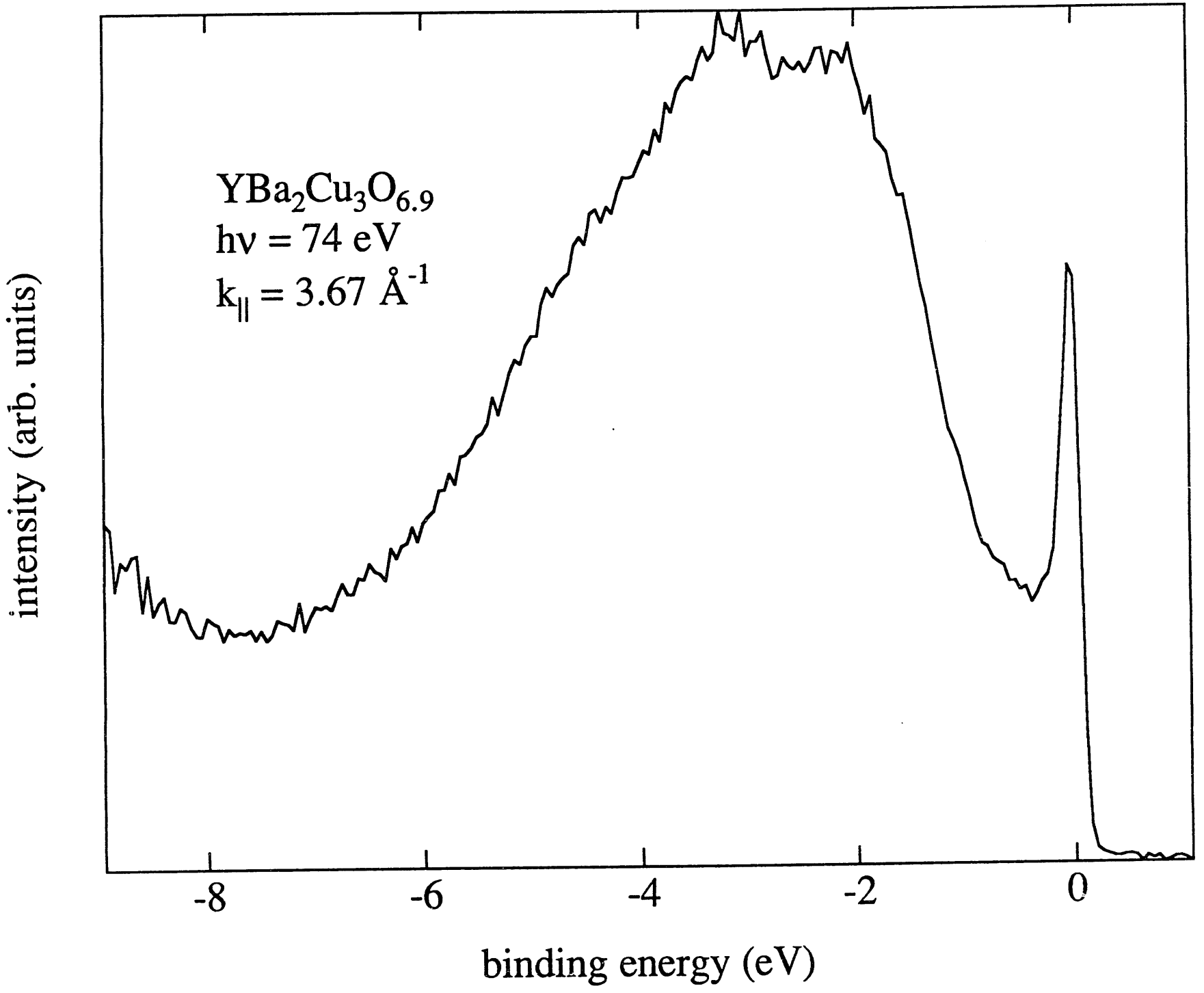
$YBa_2Cu_3O_{6.9}$
$h\nu = 74$ eV
$k_{\|} = 3.67$ Å^{-1}
intensity (arb. units)
-8
-6
-4
-2
0
binding energy (eV)

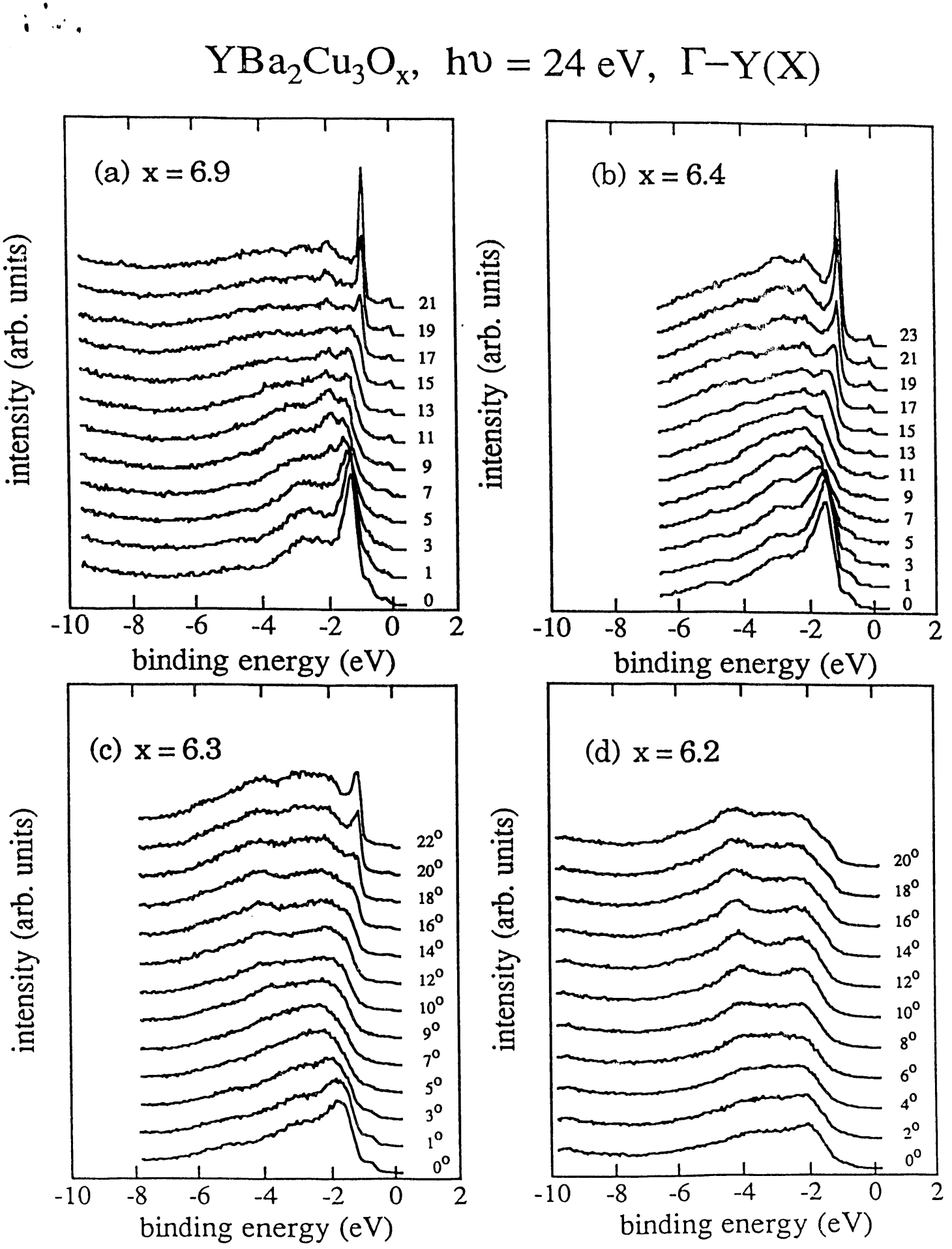
$YBa_2Cu_3O_x$, $h\upsilon = 24$ eV, Γ–Y(X)
(a) x = 6.9
(b) x = 6.4
(c) x = 6.3
(d) x = 6.2
intensity (arb. units)
binding energy (eV)
-10 -8 -6 -4 -2 0 2
21 19 17 15 13 11 9 7 5 3 1 0
23 21 19 17 15 13 11 9 7 5 3 1 0
22° 20° 18° 16° 14° 12° 10° 9° 7° 5° 3° 1° 0°
20° 18° 16° 14° 12° 10° 8° 6° 4° 2° 0°

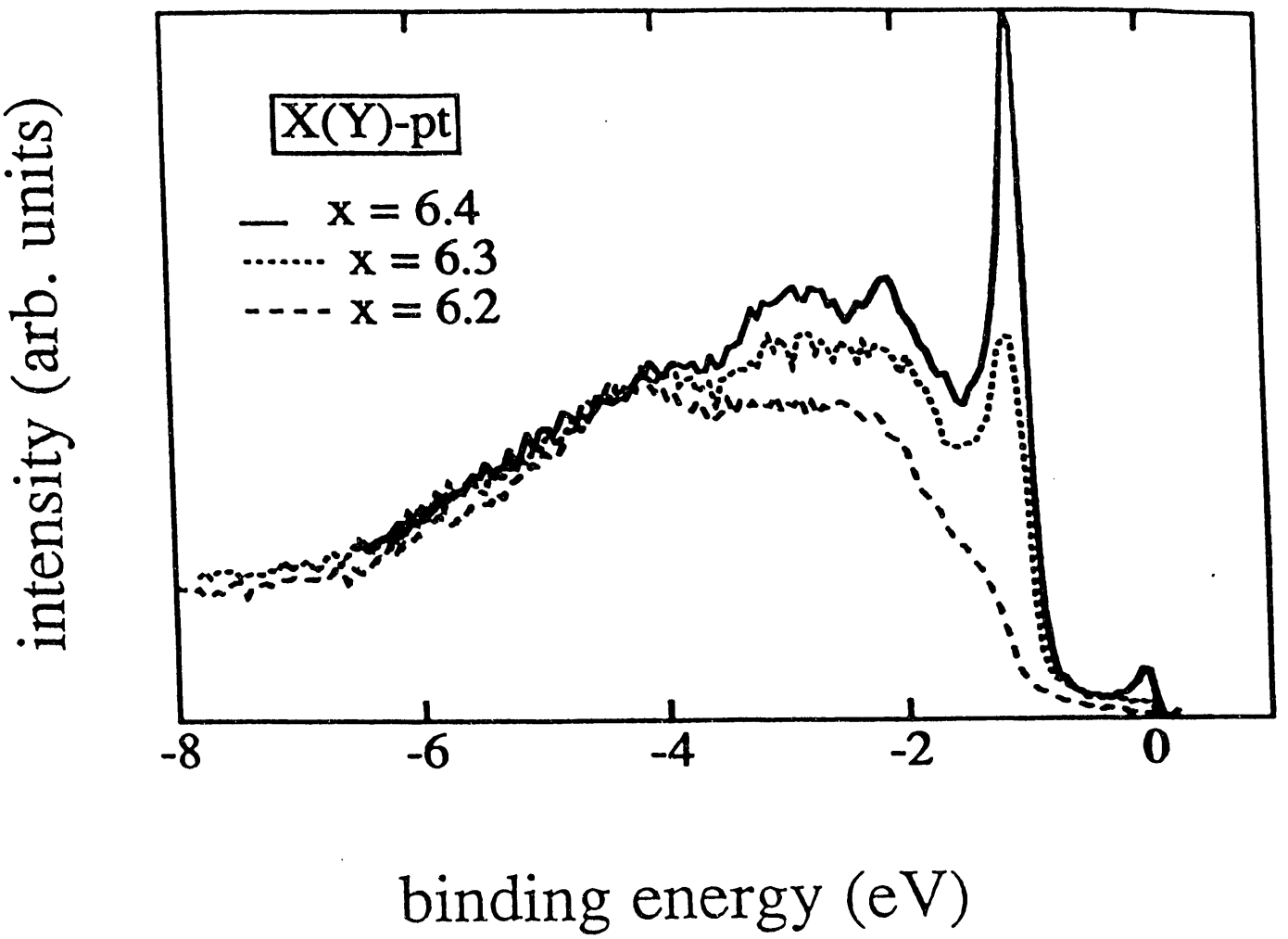
X(Y)-pt
x = 6.4
x = 6.3
x = 6.2
intensity (arb. units)
-8
-6
-4
-2
0
binding energy (eV)

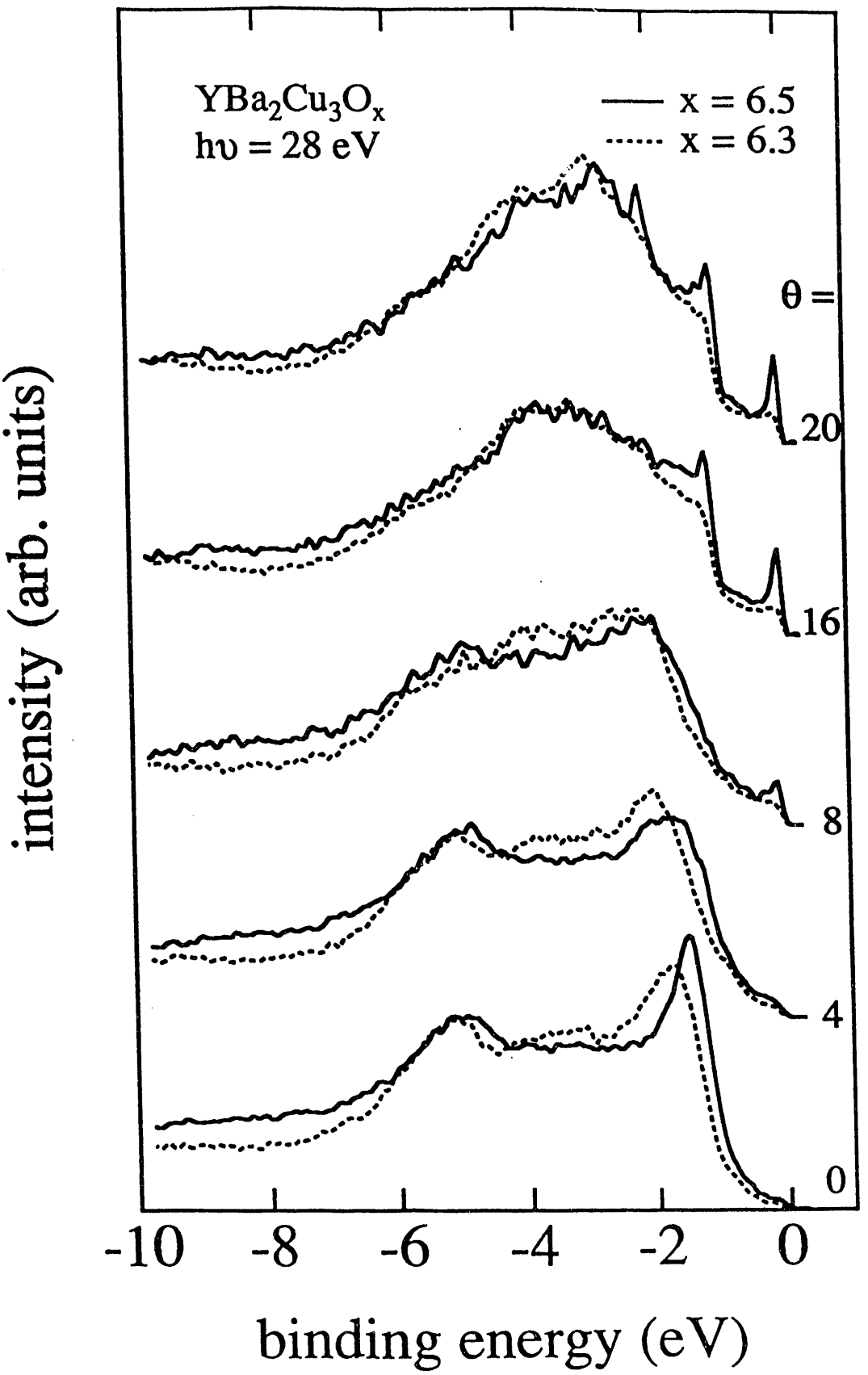
YBa2Cu3Ox
hυ = 28 eV
x = 6.5
x = 6.3
θ =
20
16
8
4
0
intensity (arb. units)
-10
-8
-6
-4
-2
0
binding energy (eV)

END

DATE
FILMED
3/5/93